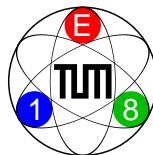# DEVELOPMENT OF A DIGITAL TRIGGER FOR ELECTROMAGNETIC CALORIMETER

by

Stefan Huber

Physik Departement E18
Technische Universität München

10.06.2010

Contents

Chapter 1

Introduction

The study of nuclear and particle physics is a very important part in understanding the basic structure of the matter. Besides the search of new particles also a deeper understanding of the already known particles and their resonance described by fundamental theories like QCD is very important.

The COMPASS experiment being able to sustain high particle fluxes and trigger rates is perfectly suited for this tasks. The high precision of the spectrometer in addition with the variety of beams which can be used for studies on a fixed target made of different materials allows to cover a broad physics program. The physics addressed in COMPASS as well as a description of the experiment can be found in chapter 2.

During the first operation with a hadron beam the possibility of measuring the pion polarisability via the Primakoff effect has been studied. Therefore a trigger based on a hodoscope and the electromagnetic calorimeter was used. Of these two triggers only the calorimeter trigger turned out to be a good candidate to use for future runs. Because in 2009 the trigger hardware was not available anymore and the analogue implementation turned out to be not perfectly reliable, a digital trigger was implemented in the existing readout electronics during 2009. The functional principle of this trigger is described in chapter 4.

The development as well as the commissioning has been done during the 2009 run. A test beam setup was used to gave a first feedback if the algorithms developed using offline data also work stably within the FPGAs used in the frontend electronics. Further improvements were done to allow transmission of the data stream used for read out in parallel to the trigger information. The final step was to attach a backplane used for final trigger decision and to tune the trigger parameters. Results of the performance extracted from the data taken in November 2009 are shown in chapter 5.

The full calorimeter will be equipped with the trigger logic latest until 2012 where a full year of data taking using this trigger is foreseen[2]. The expected rates as well as additional features which can be implemented are described in chapter 6.

Chapter 2

The COMPASS experiment

COMPASS (**CO**mmon **M**uon and **P**roton **A**pparatus for **S**tructure and **S**pectroscopy) [1] is a fixed target experiment at CERN[1]. It is located at the unique M2 beam line of the SPS (**S**uper **P**roton **S**ynchrotron) which can provide different types of beams depending on the requirements of the experiment. The beam can be adjusted to contain as primary particles muons, electrons, protons and pions with a small admixture of pions. In addition the antiparticles of each of them can be provided.

This allows to cover a wide spectrum of physics to be studied at the experiment.

2.1 The beam

The type of physics which can be studied at COMPASS mainly depends on the type of beam particles as well as on the target. The beam delivered to COMPASS is created by steering the primary SPS beam consisting of 400 GeV/c protons into the production target T6. This target consists of Beryllium of which several thicknesses can be chosen depending on the desired beam intensity at COMPASS. The beam delivered to COMPASS does not come continuous but is divided into the SPS spill cycle, where the whole cycle has a certain length which was around 40 s in 2009. This cycle is further split into injection, acceleration and extraction, where several experiments share the beam. The extraction time for COMPASS is around 10 s.

The majority of particles produced at the primary target are pions. In order to produce a muon beam out of them a 600m long decay track is introduced after selecting the pion momentum to 177 GeV/c. There the muons are produced by the decay of the pions into muons and muon neutrinos $\pi^+ \rightarrow \mu^+ + \nu_\mu$. Both the muon and the neutrino have spin 1/2 while the pions have spin 0. Due to that the muon and the neutrino always have inverse helicity compared to each other. Due to the parity violation of weak interaction

---

[1]Organisation Européenne pour la Recherche Nucléaire, European Organization for Nuclear Research

and the vanishing mass of the neutrino, the muon is produced right handed and provides a natural polarization of 75%.

After the decay line a hadron absorber is placed which consist of nine beryllium blocks each having a length of 1.1 m and so providing a total depth of 9.9 m absorbing materials which filters out nearly all hadrons. After that the muons beam is consecutive passing several toroidal magnetic collimators which select the muon momentum and the beam profile provided to COMPASS. Further the beam is passing a 250 m long transportation line to the surface where COMPASS is situated. In order to provide a good compromise between muon flux and energy the beam momentum is selected to beam 160 GeV/c.

For data taking with hadronic beams the absorbers are taken out of the beam line allowing all hadrons to pass to the experiment. The composition is mainly selected by the chosen polarity of the beam and the number of hadrons produced at the production target which did not decay until they reach COMPASS. The beam composition is shown in Table 2.1.

positive beam	negative beam
Protons 71.5%	Antiprotons 0.5%
π^+ 25.5%	π^- 95%
K^+ 3.0%	K^- 4.5%

Table 2.1: Composition of the hadronic beam.

In order to be able to distinguish the incoming particles two CEDAR detectors are placed at the end of the beam line. These Čerenkov counters can be adjusted to detect certain type of particle by selecting a proper pressure for the filling gas.

In addition to those kinds of beams for physics analysis a 40GeV/$c$electron beam can be selected by putting an electron converter into the beam line. This beam is used for calibration of the electromagnetic calorimeters.

2.2 The Targets

For hadronic beams several types of targets were used depending on the different types of physics addressed within different periods. During the test measurement in 2004 where several nuclear targets consisting of lead, copper and carbon were used to study the effect of the target material to the measurement of the Primakoff cross-section as well as for diffractive measurements.

For the precise measurement with the hadronic beam the targets were selected to exactly fulfill the desired requirements. For the study of diffractive production of exotics as well as for central production targets with low probability of multiple scattering are required.

Therefore the data taking in 2008 as well most of the data taking in 2009 was performed with a target made of liquid hydrogen LH_2. This target has a length of 40 cm.

In addition to that in the end of 2009 different segmented, solid targets were used to study different physics. To study the nuclear effects to the data taken with the LH_2 target several discs of lead were used. For the study of the Primakoff reaction two discs of Nickel were used. This material has a quite high atomic number of 28 what provides a reasonable high cross section for the reaction. Furthermore as the isotope Ni^{60} is of type spin 0^+ what decreases nuclear distortions to the measurement. In addition some tungsten discs were added for a test measurement of the π^0 lifetime.

2.3   Physics Goals at COMPASS

The physics with the muon beam addresses mainly the spin structure of the nucleons. The total nucleon spin of 1/2 has been found to be only created to a factor of 30 % by the sum of the spins of the quarks. The remaining 70 % are created by a combination of the angular momentum of the quarks in combination with the angular momentum and spin of the gluons. Therefore COMPASS tries to measure all this components with a very high precision. For the gluon polarization part Δg a process called photon gluon fusion is used which can be identified by the production of D-mesons. Further the measurements with a target polarized in transverse direction allow to measure asymmetries of the produced hadrons which allow to draw conclusions on the transverse spin distributions as well as on the angular momenta.

The physics with the hadron beams mainly focuses on the search for exotic hadrons. This are particles not described by the simple quark model which only described the mesons and baryons, but which are predicted by QCD. The search for these particles is done via the process of central production as well as with diffractive scattering where the beam particle (pion or kaon) is exited while scattering on a nucleus without destroying which stays intact. The particles which are searched for are mainly glue balls which are hadrons consisting only of a valence structure of gluons and hybrids which are combinations of gluons and quarks as valence particles.

The last main topic is the study of the chiral perturbation theory which is an effective field theory derived from quantum chromodynamics. The predictions of this theory are among others found in the prediction of values for the polarisability of mesons. This quantity can be investigated via the Primakoff reaction (Fig. 2.1) where the meson reacts via a Compton scattering process in inverse kinematics with the target nucleus. With this reaction mechanism reactions with other particles than a photon in the final state can be analyzed giving a more precise insight if the chiral perturbation theory is correct.
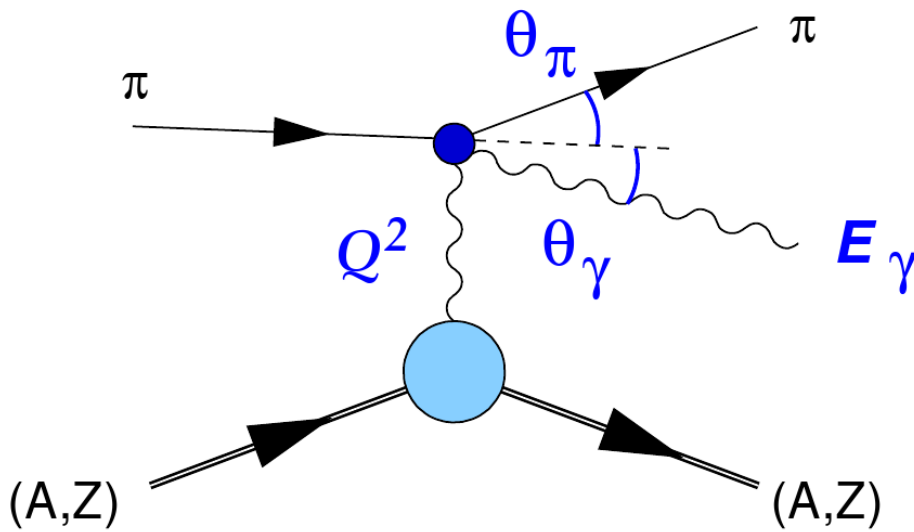
Figure 2.1: Illustration of the Primakoff reaction. [2]

2.4   The Experimental Setup

As common for most of the fixed target experiments COMPASS is set up in a linear shape. A drawing of the set up can be found in figure 2.2. In order to have a high resolution spectrometer the set up is divided in two stages: the upstream part, called large angle spectrometer LAS, and the downstream part, called small angle spectrometer. This kind of setup allows to optimize the acceptance of the spectrometer because particles with low momentum bended in the magnet of the LAS can be analyzed there while the high momentum particles are mainly bended by the magnet of the SAS and are analyzed there. This means the low momentum particles are already gone and not missed because the magnet is bending them out of the acceptance of the detectors.

2.5   Tracking Detectors

The whole length of the experiment is covered with tracking detectors. There are three groups of tracking detectors which are distinguished by their position in the set up as well as their active areas.

The Very Small Area Trackers are placed upstream of the target as well as downstream with a small distance to the target. They cover only a small distance to the beam of up to 3 cm and and serve as very precise detectors for the particles in the incoming beam and allow a very precise vertex reconstruction. The detectors belonging to this group are:
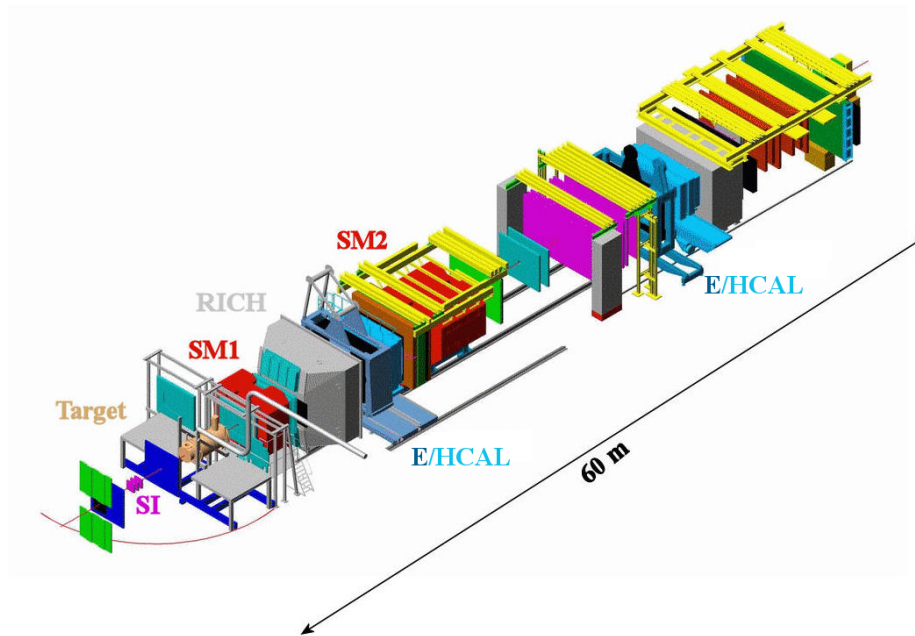
Figure 2.2: Artists view of the COMPASS spectrometer. [1]

1. The BMS (**B**eam **M**omentum **S**tations) are placed up to 100 m upstream in the beam line. These hodoscopes provide a spacial resolution between 400 μm and 2.5 mm and a timing resolution of around 500 ps. These detectors are the first ones seeing the beam particles and allow a direct measurement of the beam momentum. Unfortunately they can only be used with the muon beam because the interaction length of these detectors would cause too many hadronic interactions already in the beam line.

2. The Silicon Microstrip Detectors having the best spacial resolution of all trackers used in COMPASS are placed in the direct proximity of the target. The cover an area of 5×7 cm^2 and have a spacial resolution better than 11 μm what allows them to be perfectly suitable to be used as high precision vertexing and beam reconstruction detectors. These detectors are cooled with liquid nitrogen in order to reduce the effects of radiation damage.

3. The third type of these detectors are the Scintillating Fibre stations (SciFis) which provide a less precise spacial resolution of 130 μm but provide a very precise timing of 400 ps. For hadron data taking they are partly removed because of their high radiation length.

The Small Area Trackers area detectors are placed over nearly the whole spectrometer length providing a good spacial resolution for a region with a medium distance to the beam axis of the spectrometer acceptance.

1. The GEMs (**G**as **E**lectron **M**ultiplier) are gaseous microstrip detectors consisting of three thin insulating capton foils which are covered with a layer of copper on both sides(Fig. 2.3). Small holes area etched into the foils in order to allow the electrons to pass through. The whole volume is filled with a gas mixture of Ar/CO_2 in the ratio 70/30. A traversing particle ionizes the gas and the resulting electrons drift towards the transfer gap. A high voltage between the upper and lower foils makes an avalanche electron multiplication in the holes. After traversing the gas volume the electrons hit the readout plane which consists of 768 readout strips. For high intensity beams the central region consisting of a circular inactive area with a diameter of 5 cm has to be switched off in order to decrease the occupancy. In addition to this normal GEM detector also Pixel-GEM detectors are constructed where the central part is not read out via strips but via pixels, allowing to have the central region always switched on. The GEM detectors cover an area of 31×31 cm^2 with a spatial resolution of 70 μm.
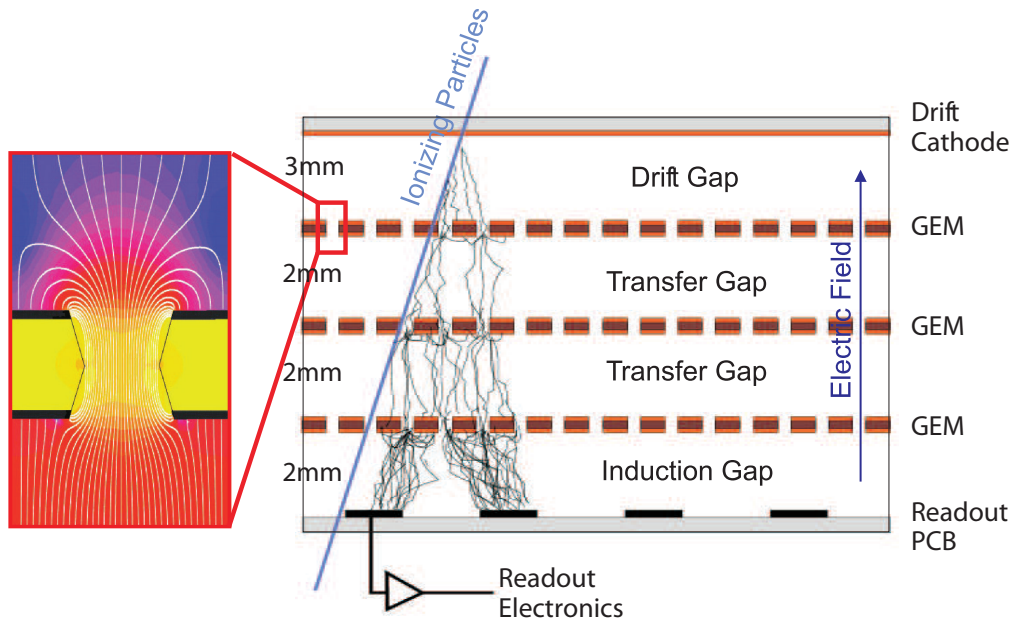
Figure 2.3: The GEM detector principle.[1]

2. The MicroMeGas (**Micro Me**sh **Gas**eous structure) are also gaseous microstrip detectors (Fig. 2.4) filled with $Ne/C_2H_6/CF_4$ in a ratio of 80/10/10. The electrons from ionization in the conversion gap drift through a micromesh towards the readout anode. The high field gradient of 50kV/m between the mesh and the anode creates an avalanche of electrons which are read out by 512 strips per detector. These detectors cover an area of 40×40 cm^2 where also the central region of 5 cm in diameter is inactive. The spacial resolution is 90 μm. The short distance between the mesh and the anode is responsible for electrical discharges which can disturb the readout signal.

Figure 2.4: The MicroMeGas detector principle.[1]

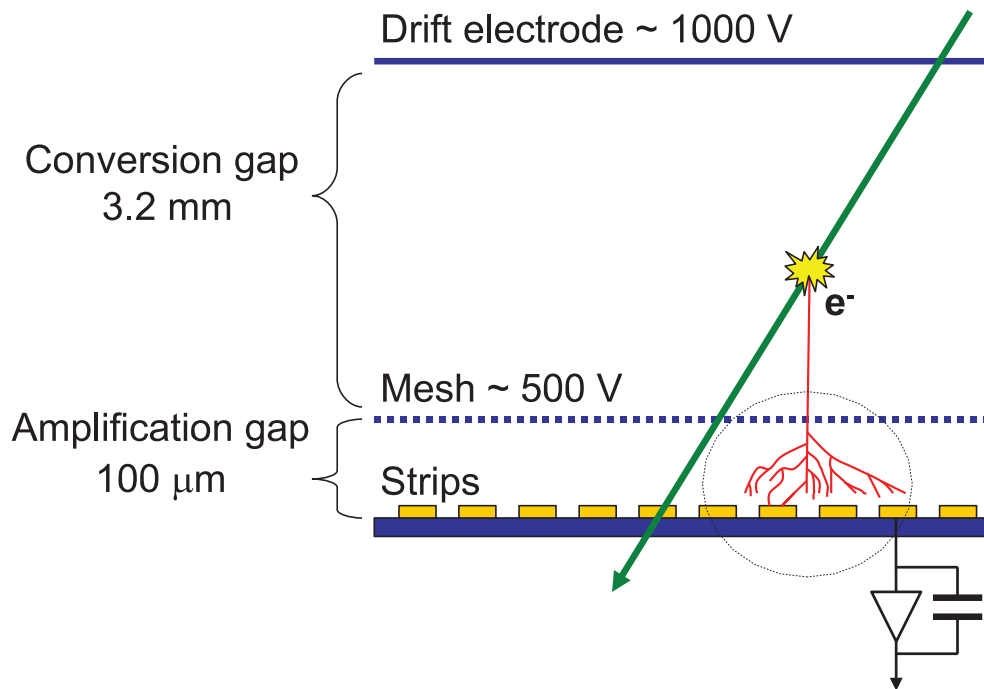To cover the bigger angles in the spectrometer acceptance the Large Area Trackers are used. These detectors have dimensions of several square meters and provide still a spacial resolution in the millimeter scale.

1. The STRAWs (Straw tube chambers) consist of several layers of thin capton tubes. They cover an area of 3.23×2.80 m^2 and are located only in the SAS. In the center of the tubes anode wires are strained while a gas mixture of $Ar/C_2H_6/CF_4$ in the ratio 74/6/20 is responsible for the gas amplification. The track position is measured as the location of the passed tube. A spacial resolution of 6.1 mm to 9.6 mm is obtained. In addition to that the drift time in the tube is used to determine the position of the track in the tube. This improves the resolution to 190 μm. In order to get a two dimensional track position three chambers in horizontal, vertical and one with an angle of 10° respectively to the vertical one are used in one station.

2. The **M**ulti**W**ire **P**roportional **C**hambers (MWPC) are equipped with 1 m long anode wires with a diameter of 20 μm and a pitch of 2 mm. For the amplification gas the same mixture as in the straw tubes is used. An electrical field between the cathode wires and the barrier of the chambers of 5 kV accelerate the electrons towards the wires and create an avalanche. The position of the track is measured as a function of the position of the closest wire without having the possibility to use time information. This reduces the maximal spacial resolution to 1.6 mm while covering an area of 1.78×1.20 m^2.

3. As the last type of tracking detector **D**rift **C**hambers (DC) are used (Fig. 2.5). They have a similar set up as the MWPC but provide additional wires connected to ground. This different structure of the electrical field allows to measure the drift time of the electrons and thus to obtain a better resolution of 190 μm. This detectors cover an area of 1.80×1.27 m^2 and are stationed in the LAS. In the SAS large area DCs are used covering 5.00×2.50 m^2 with a reduced spatial resolution of 500 μm.
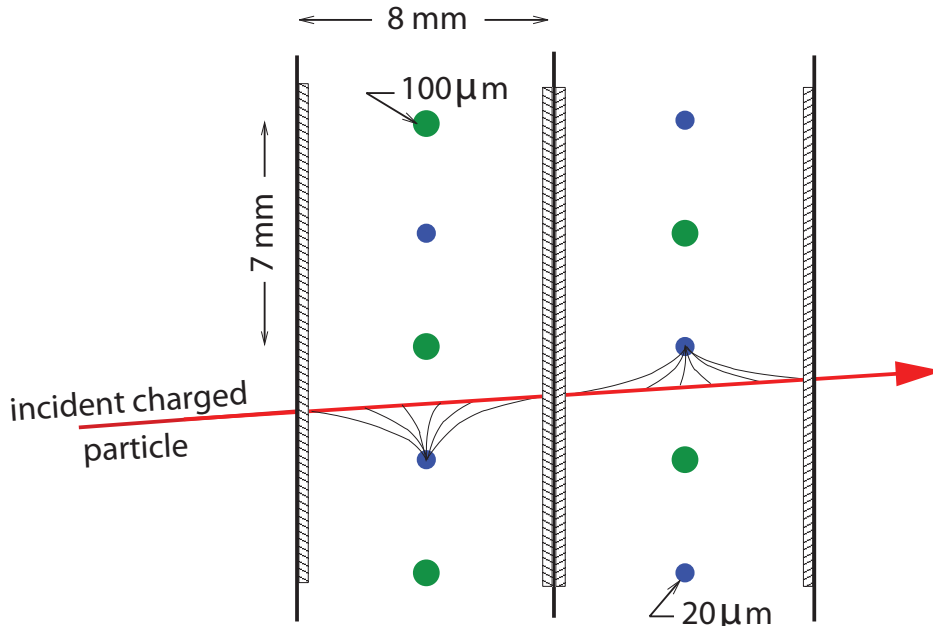

Figure 2.5: The DC detector principle.[1]

2.6   Particle Identification

COMPASS uses four different kinds of detectors for particle identification. These are necessary in order to distinguish different types of hadrons as well as to identify muons.

1. In the LAS a big RICH detector (**R**ing **I**maging **CH**erenkov) is placed with dimensions of 3.3 m $\times$ $\times$ 6.6 m$\times$ 5.3 m (Fig. 2.6). As medium C$_4$F$_{10}$ gas with the high refractivity of n = 1.0015 is used. Particles traversing the volume with a speed greater than the speed of light in that medium emit Cerenkov radiation under an angle defined by $\theta_C = \frac{1}{n \cdot \beta}$. This radiation is reflected back via a wall of mirrors to the light sensitive focal plane where, depending on the angle, rings are measured. These rings correspond to the Cerenkov angle and thus to the speed of the traversing particle. By measuring the momentum of the particle with the tracking system the mass and thus the type of the particle can be measured. Hadrons having a momentum between 5 GeV/c and 43 GeV/c can be identified.
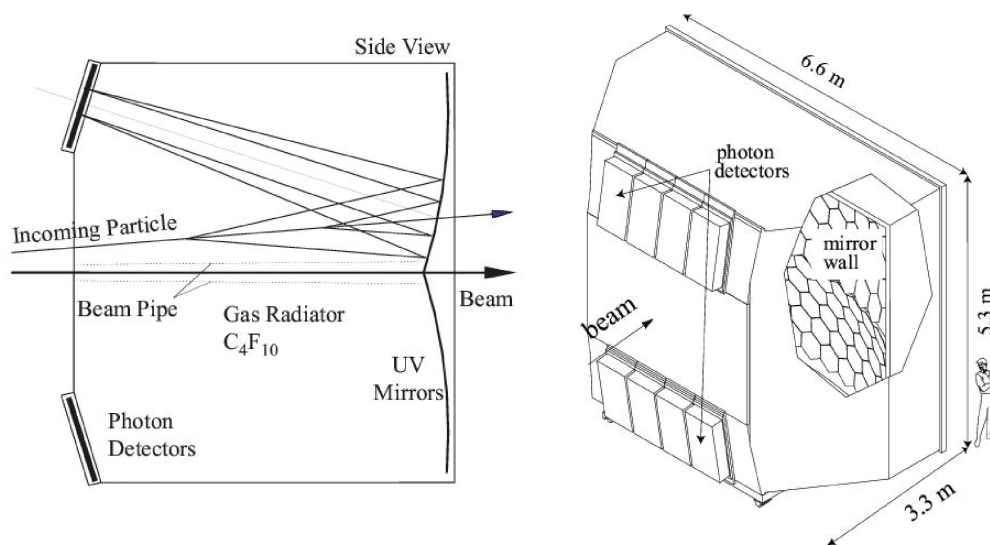
Figure 2.6: Detector principle of the RICH and sketch of the setup.[1]

2. In front of the target another type of detectors is placed which take advantage of the Cerenkov effect. This detectors are the two CEDARs (**CE**renkov **D**ifferential counters with **A**chromatic **R**ings) in which the refraction index can be adjusted via the pressure. The emitted light is focused via mirrors and lenses onto the focal plane as well as it is corrected for chromatic aberration. The light sensitive detectors are placed at a certain radial distance being sensitive to one special emission angle which corresponds at a fixed particle momentum (beam momentum) to a certain particle. Combining the information of both detectors allows to clearly distinguish pions from kaons in the beam.

3. For measurements in the hadron program a **R**ecoil **P**roton **D**etector (RPD) is installed surrounding the target. This detector consists of two layers of scintillators with a relative distance of 655 mm. The detector is used as a trigger component for diffractive scattering on the one hand and also as a particle identification system for the protons. This is done by measuring the time of flight of the recoil particles between the two scintillator layers providing the speed of the particle. The recoil momentum is measured via the angles in which the proton is traversing the detector. The correlation between this two values identifies the type of particle.

4. In order to effectively identify muons several layers of absorber material is placed at the end of both detector stages. This material are the electromagnetic and the hadronic calorimeters as well as specially installed concrete or iron walls. Nearly all hadrons as well as the light leptons are stopped in this absorber material while the muons are passing through as minimum ionizing particles. All particles detected afterwards are assumed to be muons. These are measured via so called muon walls consisting of different types of drift tubes arranged in several layers and provide a spacial resolution in the millimeter range.

2.7   The Calorimeters

For each of the two spectrometer stages COMPASS has a separate electromagnetic calorimeter as well as a hadron calorimeter. These detectors are named with ECAL1/HCAL1 and ECAL2/HCAL2. While the hadron calorimeters are both sampling calorimeters the electromagnetic calorimeters mainly consist of homogeneous detector cells made of lead glass. Only the central part of ECAL2 where the occupancy and the radiation dose is the highest is equipped with sampling blocks of Shashlik type.

2.8   Detection of Particles in Calorimeters

Whenever a particle hits some detector material it does some type of interaction depending on its charge, mass, momentum and particle type.

Leptons as well as photons mainly react via the electromagnetic interaction which allows several dominant processes. Due to the high momentum of the particles in COMPASS the low energetic effect like compton scattering or the photoelectric effect can be neglected when one considers the energy loss in the calorimeters. The dominant processes are Bremsstrahlung for leptons and pair production for photons. In the pair production process the photon with an energy above 1022 keV converts into an electron and a positron-while passing a nucleus while bz Bremsstrahlung the electrons emitt photons due to the influence of the nuclear electric field.

High energetic particles in a medium undergo continuous energy loss by consecutive interactions via these two processes. More and more electrons, positrons and photons are created by that. This is called the electromagnetic shower. As soon as the critical energy E_c is reached the Bremsstrahlung becomes less important than ionization losses and the shower process stops. This critical energy is a constant depending on the material of the detector cell. For lead glass of the type a typical critical energy is 17 MeV.

The energy lost by Bremsstrahlung is described by an exponential law eq. (2.1) with the material constant X_0 called the radiation length.

$$(2.1) \qquad\qquad E(x) = E_0 \cdot \exp\left(-x/X_0\right)$$

In order to stop photons completely the electromagnetic calorimeters have to be several radiation lengths deep. For example the lead glass type TF01 used for the GAMS blocks has a radiation length of X_0=2.7 cm With a total depth of 45cm they have a length of 16 radiation lengths. That means only a negligible fraction of around 10^{-5}% of the energy of the photons is not detected that corresponds to 22 keV at a photon energy of 200 GeV.

While the energy loss of the particles strongly depends on their mass havy particles like muons and hadrons pass through the detector material as minimum inoinzing particles and deposite only a small amount of their enery into the detector.

Hadrons can in addition interact via the strong interaction with the nuclei of the absorber material. The characteristic quantity is the nuclear interaction length λ_a describing analogous to the radiation length for electromagnetic interactions the energy loss of hadrons due to the strong interaction as seen in eq. (2.2).

$$(2.2) \qquad\qquad E(x) = E_0 \cdot \exp\left(-x/\lambda_a\right)$$

Thus for stopping the hadrons additional material in the hadronic calorimeters allows the measurement of the energy deposited in the hadronic showers.

2.9 Electromagnetic Calorimetry

COMPASS is equipped with two electromagnetic calorimeters, one for each stage. Electromagnetic calorimeters used to determine the energy of electromagnetic interacting particles are important to identify neutral particles which are not seen by the tracking detectors. That means the main type of particles for which the detection in the electromagnetic calorimeter is needed are photons. Having knowledge about the hit position of the photonsand their energy one can trace them back to their vertex and can reconstruct intermediate particles like π^0 from $\pi^0 \rightarrow \gamma + \gamma$. The electromagnetic calorimeter in the first stage of the spectrometer ECAL1 consists of three different types of lead glass modules taken from previous experiments. They are called MAINZ, OLGA and GAMS.

The electromagnetic calorimeter in the second stage of COMPASS, ECAL2, consists of 3068 cells arranged in a matrix of 64×48 cells with a small hole in the center which has the dimension 4×4. Each of these cells has a square surface with a side length of 3.8 cm, the depth of each module is 45 cm. The center of ECAL2 is equipped with sampling calorimeter cells of so called Shashlik type, the outer parts consist of lead glass modules of the GAMS type where the more central cells are radiation hard(Fig. 2.7). ECAL2 has an energy resolution of

$$(2.3) \qquad\qquad \sigma(E)/E = (59.4 \pm 2.9)\%/\sqrt{E} \oplus (7.6 \pm 0.4)\%.$$

2.9.1 Detection in the Lead Glass Cells

The lead glass detector elements are continuous transparent blocks. High energetic electrons and positrons from the electromagentic shower emit Cherenkov radiation while passing through the material. The emitted photons are collected at the end by photomultiplier tubes where they are converted into an electrical signal. The number of Cherenkov photons is proportional to the energy deposited by the particle.

Figure 2.7: All three types of detector cells used in ECAL2.

2.9.2 The Shashlik Detector Cells

In contrast to the continuous cells the Shashlik type is a segmented construction made of consecutive layers of plastic scintillators and lead absorbers in which the showers are created. The light created in the scintillator layers is transmitted via wavelength shifting fibres to a photomultiplier tube where it is read out.

2.10 The Hadronic Calorimeters

That means in case of the COMPASS around 80% of the hadrons deposit already a significant amount of energy in the electromagnetic calorimeters. The rest of the energy has to be detected afterwards in the hadronic calorimeters. They are sampling calorimeters consisting of steel absorbers with a thickness of 2 cm for HCAL1 and 2.5 cm for HCAL2 where the hadronic showers are building up. In between there are always 5 mm of scintillator material from where the light is transported by wavelength shifting fibers to photomultiplier tubes. The depth of the hadronic calorimeters is around five nuclear interaction lengths where simulations have shown, that most of the hadrons with energies between 10 GeV and 100 GeV are stopped. The energy resolution for the hadron calorimeters is not as good as for the electromagnetic calorimeters and is described by

(2.4) $$\sigma(E)/E = (59.4 \pm 2.9)\%/\sqrt{E} \oplus (7.6 \pm 0.4)\%.$$

2.11 The Trigger System at COMPASS

The purpose of the trigger system is to start the readout of the COMPASS spectrometer for events which fulfill a certain trigger condition matching to the type of events to be studied. All other events are immediately rejected.

The trigger system at COMPASS consists of a first level trigger and an online filter called CINDERELLA. The first level trigger has to be set in such a way that the event rate is compatible with the individual detector subsystems as well as the amount of data which can be handled by the DAQ (**D**ata **AcQ**uisition). The trigger rates which can be handled right now are between 20 kHz and 30 kHz depending on the trigger type and the included equipment.

The online filter can be used to reject events or detector signals of the events which were already recorded in order to reduce the amount of data which has to be stored. This is necessary due to the quite high costs for storing on the tapes at the **C**ERN **A**dvanced **STOR**age manager (CASTOR).

The trigger decision has to be ready within a certain time interval limited by the read-out buffers in the frontend electronics. This trigger latency is around 500 ns in the pure analogue trigger set up while the implementation of the digital ECAL2 trigger required a trigger time shift by additional 700 ns. This total latency of 1.2 μs is close to the limit of the equipement with the smallest buffer sizes, the F1 TDCs.

2.12 Detectors Used for Triggering

In the trigger system two kinds of detectors are used. On the one hand there are elements which react on a certain physics signature and give a positive trigger signal while on the other hand a veto system is installed. The veto system consists mainly of hodoscopes rejecting events which are induced by the beam halo or for which a part of the scattered particles are not within the spectrometer acceptance. In addition there is also a beam killer system vetoing on not scattered beam particles.

For the muon programm a large set of hodoscoped is placed over the experiment, mainly behind the muon filter system. For interactions with $Q^2 > 0.5(\text{GeV/c})^2$ the trigger set up is purely geometrical. That means the trigger condition is based on the coincidence of two regions in two different hodoscopes, selecting a certain scattering angle.

For small scattering angles at small Q^2 this coincidence is prone to background events. Therefore in addition a certain energy deposition in the hadronic calorimeters is required.

For the hadron spectroscopy the triggering on muon tracks is not useful anymore. Therefor a different trigger scheme was chosen optimized for the different physics cases. The recoil proton detector surrounding the target is used to trigger on events, in which the scattering of the beam particle transfers enough energy to the target protons to accelerate them out of the target volume. In addition to that a multiplicity counter is placed downstream of the target which selects events with at least a certain amount of outgoing particles. This detector has a central hole in front of which a small scintillating disc is placed which is sensitive to particles scattered under small angles.

For the events mainly containing neutral particles with low Q^2, the Primakoff trigger, selecting a certain energy deposition in ECAL2 which was developed during this work, is used.

2.13   The Data Acquisition System

The required performance of the spectrometer from the point of view of data rates has to be supported by a capable **D**ata **A**c**Q**uisition system (DAQ). This starts with the frontend electronic which is responsible for the gathering of the data directly coming from the detectors. Several types of electronic boards are used for the different detectors. For example there are several different types of sampling ADCs [2] used for reading out detectors like calorimeters, silicon and GEM detectors and the RICH [5]. Further there are also boards equipped with TDCs[3] to read out detectors which provide data as a time information like DCs and the hodoscopes.

In order to transmit the information coming from the detectors with as less cables as possible, concentrator modules are placed next to the frontend. This modules can combine the data via several input connectors and prepare them for further transmission. The modules used here are the GeSiCAs[4] and the CATCHes[5]. This modules have an attached S-Link[6] transmitter card which are connected to the readout computer via optical fibers. The maximum possible bandwidth of these modules is 160 MByte/s.

This data is received in a two stage computing network based on the DATE framework developed for the ALICE experiment at the LHC. The first stage consists of the **R**ead**O**ut **B**uffers (ROBs) which receive the data and store them temporary in their memory. As soon as all data for one event is accumulated at the next stage, the eventbuilder PCs receive the data and form one data block out of all the data and store them as binary file. This files are stored later on the storage tapes at CASTOR.

The data received with the eventbuilders is passed through an additional computing stage, the online filter CINDERELLA. There the data is checked for integrity and mon-

---

[2]**A**nalog to **D**igital **C**onverters
[3]**T**ime to **D**igital **C**onverters
[4]**GEM** and **Si**licon **C**ontrol and **A**cquisition module
[5]**COMPASS** **A**ccumulate **T**ransfer and **C**ontrol **H**ardware
[6]**S**imple-Link

itoring data is extracted. In addition there is the possibility to activate certain filtering mechanisms which exclude unwanted data from the recording procedure.

In order to perform the readout synchronous on all detectors the **T**rigger **C**ontrol **S**ystem (TCS) [4] is used. This system generates a low jitter global clock of 38.88 MHz which is transmitted to all frontend electronics. Further the system provides information which is needed to identify the event later. This is for example the event type, the event number and also the trigger bit. The trigger signal is transmitted to the detectors synchronously with the TCS clock signal what allows to reconstruct the time of the detector signals by comparing it with the trigger time which is measured relatively to the TCS clock. This quantity is called the TCS phase.

Chapter 3

The MSADC Readout System

In order to provide a flexible readout system many detectors in COMPASS are equipped with sampling ADCs. The main feature of this kind of readout is that it provides full information about the signal shape. This allows us to perform important tasks like an effective zero suppression in hardware as well as detailed pulse shape analysis in offline reconstruction.

3.1 The ADCs

In 2008 the readout of the inner part of ECAL2 was upgraded to developed ADC modules, the MSADC (**M**ezzanine **S**ampling **ADC**) [6]. This upgrade was finalized in 2009 connecting the whole detector to this readout system.

The carriercard is a 9U VME module combining four mezzanine cards shown in Fig. 3.1, i.e. 64 detector channels. The value 9U describes the height of the module in rack units (1U = 4.4 cm). The abbreviation VME stands for Versa Module Eurocard. It is a bus standard developed in 1981 providing a bandwidth of up to 80 MB/s. The carriercard does not communicate via the VME bus but uses the crate standard for housing, cooling and power supply. In addition the carriercard is connected to the VME P2 connector allowing eight carriercards to communicate with one common backplane card providing additional functionality.

On the mezzanine card four ADC chips of the type ADS5270 produced by Texas Instruments are placed. Each of them has a maximum sampling frequency of 40 MHz and a 12 bit resolution. The number of inputs to one ADC is eight, so the maximum number of channels read out by one card would be 32 with a sampling rate of 40 MHz. In our usage we want to have a 80 MHz readout. This frequency is reached by connecting one channels to two different ADCs which are operated in interleaving mode. The both ADCs are read out with two 40 MHz clocks which have a phase difference of $180°$. Due to the fact that the ADC chips have slightly different physical parameters, each of them has a different baseline which has to be corrected afterwards.
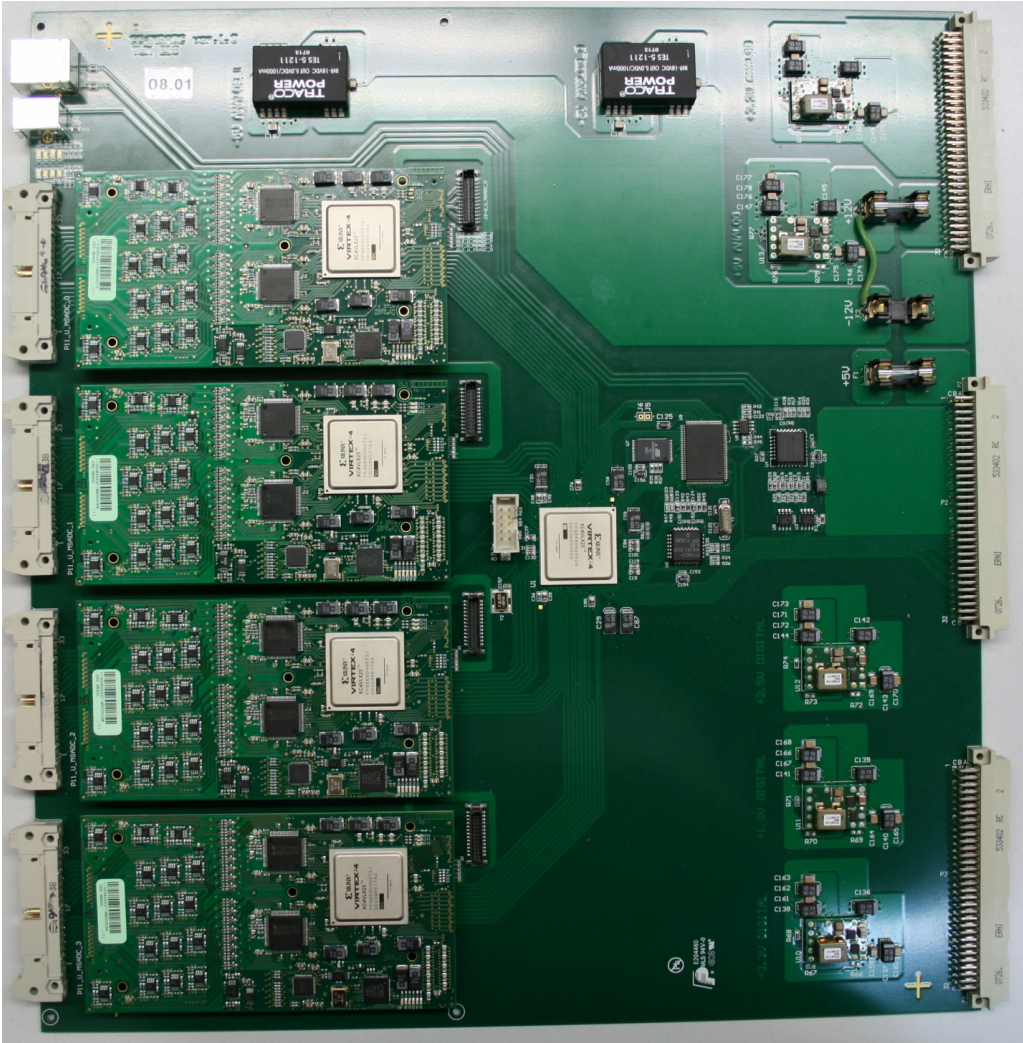
Figure 3.1: Carriercard fully equipped with four mezzanine cards (MSADCs)

3.2   The Virtex4 FPGA

FPGAs (**F**ield **P**rogrammable **G**ate **A**rrays) are integrated circuits which provide certain logic gates like AND or NOT as well as memory elements like flipflops and block RAMs. These elements are arranged in logic blocks which can be freely connected by the user using a programming language like VHDL (**V**HSIC[1] **H**ardware **D**escription **L**anguage) or Verilog. With these programming languages each used connection within the chip is described and doing that the logic is implemented. In addition to the basic operations, the FPGA manufacturers provide certain IP-cores (intellectual property cores). These are either provided as so called soft-cores consisting of code, which can be used within the chip, as well as hard-cores, which are fixed areas in the chip serving a special purpose and can be used by just connecting them to the desired logic. These cores are used for example for memory elements or clock generators as well as for more complex math operations like divisions.

On the carriercard as well as on the mezzanine card one FPGA of the Virtex-4 family (XC4VLX25-10FF668) from Xilinix is used. Inside this chip one of the most important features is the flexible clock generation provided by the digital clock managers (DCM). This IP-cores allow convert incoming clocks to other clocks with different frequencies. The clock frequencies are limited by internal chip parameters and depend on the incoming clock. For an incoming clock of 40 MHz as it is used for the MSADC cards the frequency range is 2 MHz up to 210 MHz by using one DCM. Using an additional DCM the maximum outgoing frequency would be limited by the chip itself and would have a value of 400 MHz. For the MSADC system a maximum frequency of 160 MHz is used for the interface between mezzanine card and carriercard. A possible interface running at 320 MHz was tested but turned out to be not feasible. The reason for that is accumulating jitter after each DCM. For instance using a generated 80 MHz clock from one DCM has a jitter of up to ±200 ps while the DCM for generating higher frequencies only tolerates a maximum jitter of 173 ps. Further also the phase of the outgoing clock relative to the incoming can be adjusted during run time or with a fixed value. In order to do that a feedback connection is used. This feedback line is connected to the outgoing clock with the same frequency as the incoming one (Fig. 3.2). The phase of the outgoing clock is adjusted in a way that the feedback matches to the incoming clock. By implementing so called tapped delay lines in front of the reference clock or the feedback clock the ratio can be adjusted in multiples of 75 ps corresponding to the length of one tap. By doing so the phase can be adjusted up to ±7 ns. For clocks with a phase longer than 7 ns like the 25 ns for a 40 MHz clock, there are special outputs corresponding to a phase shift of $0°$, $90°$, $180°$ and $270°$. By that a full coverage of the possible phase relations with a resolution of 75 ps is possible.

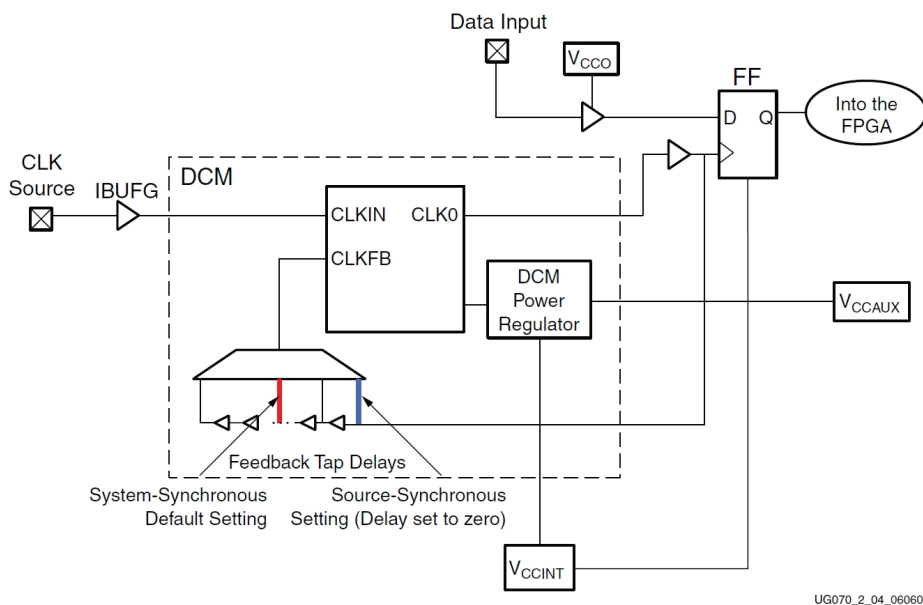[1]**V**ery **H**igh **S**peed **I**ntegrated **C**ircuit

Figure 3.2: Very rough schematic of the delay elements in a DCM. Taken from [7].

3.3   The Readout Chain

The analogue signal coming from the PMTs has a very short pulse width. This would require a samping at a very high frequency what would be only possible at limted accuracy. In order to be able to digitize this it the signal is fed to shaper cards where each of them can handle 32 channels. There the pulse is transformed in a way that it has a fast rise time between 50 ns and 62.5 ns and a long tail after reaching the peak value. The signals are fed via ribbon cables to the ADC modules. After digitization the data is transmitted via differential serial connections into the data processing FPGA where several tasks are performed.

In the first stage the data of the ADCs has to be interleaved what is done by alternating reading the data from the two ADCs with the internal 80 MHz clock of the FPGA. In order to provide synchronization between the internal clock of the FPGA and the clock coming from the ADCs an asynchronous FIFO buffer is used. This buffer which consists of a block RAM stores the data consecutively to certain memory blocks with the ADC clock and is read with the FPGA clock a few clock cycles later.

After that the pedestals are calculated at the beginning of each spill and the data is corrected by them in order to have a fixed baseline of 50 ADC channels. Further the data is stored in an additional buffer in order to compensate for the trigger latency. This buffer has a depth of around 114 clock cycles corresponding to 1.5 μs.

Finally if a trigger is received the data is stored into a ring buffer where it is stored in blocks of a certain amount of samples per trigger. The current number of samples is chosen to be 32 in order to be able to handle pile up. There are considerations to decrease

this number to maybe 24 what seems to be enough to cover all possibilities. As soon as the previous event is completely processed and transmitted, the current event is read and further processed. The processing consist of formatting the data into 32 bit words with additional headers as well to perform zero suppression. This is needed to reduce the amount of data which has to be transmitted and to be stored to only the information that has physical meaning.

At the end the data is multiplexed on the and transmitted to the readout computers.

3.4 The Data Format and Data Acquisition

The data is formatted into blocks of 32 bit words which start with the S-Link begin marker "0x00000000" and the S-Link end marker "0xcfed12000". The first block containing information is the S-Link header containing information about the event itself and the source ID of the equipment.

0	Tr. type (5)	Source ID (10)		Event size (16)	
0	Spill no.(11)		event no. (20)		
0x0000				TCS error byte	0x01 (8)

Table 3.1: The header of the SLINK protocol

The data of every SrcID delivered from the GeSiCA module is divided into smaller sub blocks depending on the equipment used. For the MSADCs the format is shown in table 3.2.

ADC header

1	ext.	Port(3)	ADC ID(2)	Err(1)	Size (12)	event number (12)

Channel header

01	chan.ID(4)	0	# samples(9)	sum(16)

Data

CTRL	extra (6)	data1 (12)	data0 (12)

Table 3.2: The MSADC data format

The ADC header is stored for every mezzanine card and contains the information if the readout is in extended sparse mode or not (ext. bit), currently this is the only mode used for reading the MSADCs. If this bit is not set the data is read out in latch all mode without zero suppression and a different data format. In the following bits the GeSiCA port (0-7) and the ADC ID (0-4) describing which mezzanine card it is are encoded. The err. bit contains the information if the buffer on the mezzanine card was in overflow. Size gives

the number of 32 bit data words for this card including headers while the event number describes the LSB of the event number also given in the SLINK header and in that way gives the information if triggers were lost for this special equipment.

The Channel header only sent, when there is data on the corresponding channel describes the channel number on the mezzanine card and the number of samples extracted from this channel. The data contained in sum are not used.

The data is formatted into two bits used for consistency checks stored in CTRL which is '01' for the first data word and '10' for all the others. The following six bits (extra) were fixed to zero but are now used to encode extra information about the amplitude found by the trigger system after, further two times 12 bit of data are stored.

The encoding of the extra word is a bit more complicated and will be explained here. The information encoded contains of the amplitude in a 11 bit value and also the sample in which the signal has been found is encoded into the format of the encoding. If the time corresponds to the first sample then the first six bit of the extra information look like '111000'. After that two times six bit are sent out containing first the least significant bits of the amplitude and then the most significant bits. In the case the time corresponds to the second sample, the first six bit consist of three LSB of the amplitude information and then '111'. After that again the amplitude is encoded from LSB to MSB. The two different cases are shown in table table 3.3.

Case1: first sample

1	111	000	Data1 (12)	Data0 (12)
10	Amplitude (6 downto 1)		Data1 (12)	Data0 (12)
10	'1'+Amplitude (11 downto 7)		Data1 (12)	Data0 (12)

Case2: second sample

1	Amplitude (3 downto 1)	111	Data1 (12)	Data0 (12)
10	Amplitude (9 downto 4)		Data1 (12)	Data0 (12)
10	'0001'	Amplitude (11 downto 7)	Data1 (12)	Data0 (12)

Table 3.3: Encoding of the extra words

3.5   Programming and Configuration of the FPGAs

The configuration can be done by manually reading and writing the I^2C registers via a program called "rw_i2c_reg". For longtime usage this is done via the "config_server" where the registers can be configured via a database and one has only to specify the task to be done. Without knowing the exact procedure the user can perform the command LOAD -A to perform all possible tasks, what means for setups without the digital trigger

to reprogram the GeSiCA (LOAD -g), the MSADC and carriercard FPGAs from the flash memory (LOAD -z) and to configure the registers (LOAD -R). For setups with the digital trigger this is extended to reprogram the backplane (LOAD -b), the calibration registers for the trigger (LOAD -c) and the CFD settings (LOAD -D). In addition the command LOAD -M is introduced which allows to read trigger monitoring parameters.

During the run it turned out, that the way the commands issued to reprogram the FPGAs did not match the requirements from the hardware. This resulted in an unreliable loading procedure which quite often failed. For the 2010 run this loading procedure has been improved and adapted in a way that the hardware can be reloaded without errors. This procedure works in the following way:

1. Loop over all carriercards and:

   (a) Send the reload command for all mezzanine cards

   (b) Check if reload command was successful:
      - Try to the pattern 0xabcd to the test register 0x0100 on all mezzanine cards
      - Check if the writing was successful
      - If yes than the reloading did not start
      - Do 5 additional tries, otherwise show an error message

   (c) Send the reload command for the carriercard:
      - Check if the carriercard is present reachable from the GeSiCA
      - If it is still present check it 10 more times
      - If it is still present retry this procedure 5 more times
      - Otherwise show an error message

2. Check every second if the carriercards come back from reloading

3. If the carriercards are not reachable after 30 seconds show an error message

4. Loop over all carriercards and check if the mezzanine cards are again reachable by trying to write 0x1234 to register 0x0100

5. If they are not reachable after 20 seconds show an error message

To program the flash memory a tool called sadcvme is used. This program uses the VME bus to transfer data via the GeSiCA to the ADC cards. The programming has to be done sequentially for each carriercard. During 2009 also the programming of the mezzanine cards had to be done sequentially what changed with an upgrade of the procedure during the run preparation for 2010. Now also a broadcast command is available. The program always gets three parameters where the first is the VME address of the GeSiCA which is adjusted there via a rotary switch. Then I^{2}C port has to been set twice which is simply the port on the GeSiCA where the ADC is connected to. The last parameters depend on what you want to do. The parameter -d# adjusts the destination where # ranges from 0

to 4 corresponding to the carriercard and the four mezzanine cards, -dff dresses all the mezzanine cards, one after the other. Instead of -dff also -b can be used to access the carriercards in broadcast mode. With an additional command of -p <file> a certain file is loaded into the flash bank of one of the cards. This can be loaded afterward with the command -r1 into the FPGA. It is also possible to load the firmware from bank zero with the command -r0 but this firmware can only be programmed via USB.

Chapter 4

The Digital Trigger System

4.1 Pedestal Subtraction

As mentioned in section 3.1 the combination of two ADCs per channel introduces two baselines per channel, which can be many ADC channels apart. Due to this the signal shape becomes quite distorted (Fig. 4.1). To be able to make a good signal shape analysis one has to know the baseline values and subtract them from the signal. This was done for offline analysis by averaging over the first even and odd samples in every pulse, four samples each. This is possible, because the latency was adjusted in such way, that those samples only contain baseline despite of pile up. This method has two disadvantages, first averaging over only a few samples introduces statistical errors in determining the baseline. Further pileup in this first samples can make the determination absolutely impossible. In order to make signal analysis online in the FPGA where we take all samples into account, without knowing if they are introduced by a physical hit in the calorimeter, the baseline has to be known in advance. In compass there is a very nice possibility to determine the baseline. Due to the fact, that the beam comes in spills with 10 seconds of beam and 30 seconds without beam the baseline can be determined by averaging over certain samples in off spill time. In the current implementation 2048 samples are used for even and odd samples. For the trigger system this baseline is simply subtracted from the samples resulting in a baseline of zero taking into account underflow by setting those samples to zero. For the data connected to the readout the pedestals are subtracted from the data adding an offset of 50 to keep some information about the behavior if the signal gets negative. This fixed baseline of 50 simplifies the analysis of the offline data as now the per event determination of the baseline can average over eight samples not distinguishing between even and odd. Also huge deviations from the baseline give some hint to pile up.
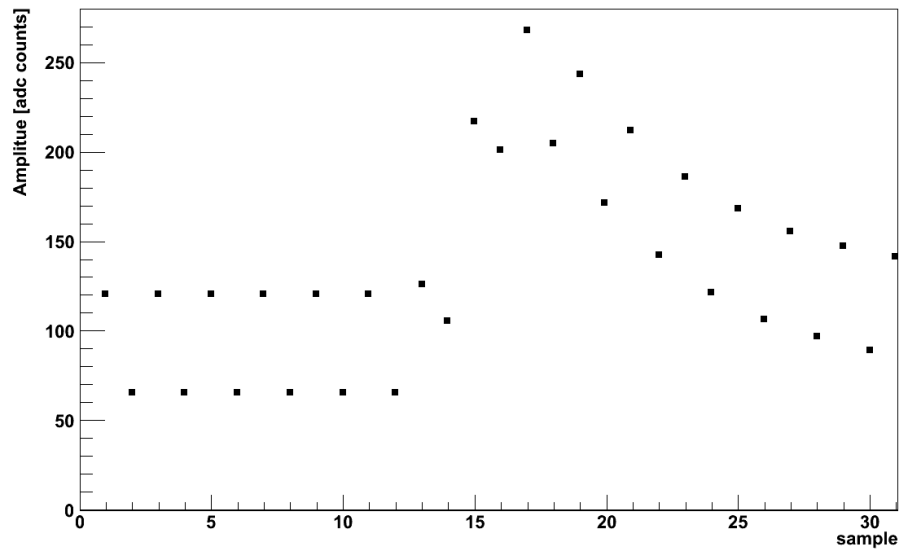
Figure 4.1: Sample pulse recorded with ECAL2 without pedestal subtraction. Clearly visible are the two different baselines which are 55 ADC channels apart in this case
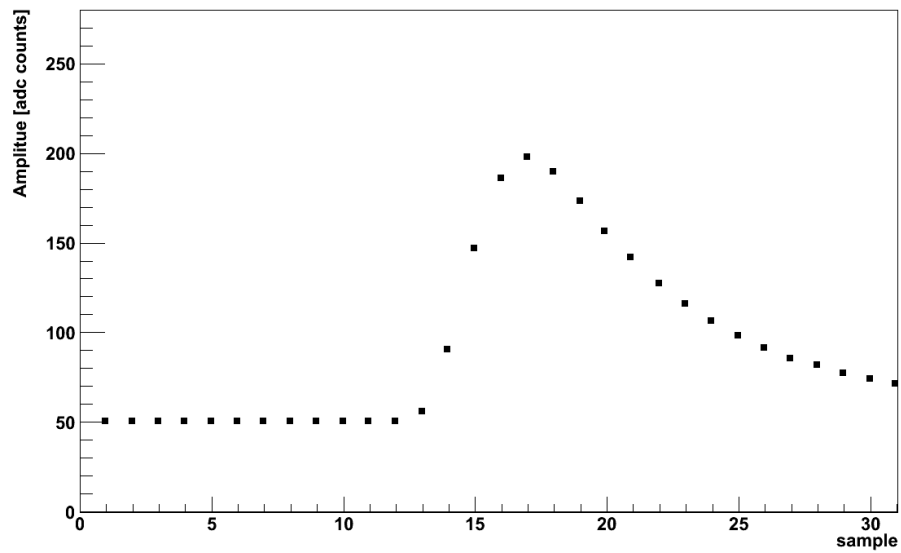

Figure 4.2: Sample pulse recorded with ECAL2 after pedestal subtraction. Baseline fixed to 50 ADC channels

4.2 Signal Detection and Time Determination

The main part of the trigger algorithm is the detection of physical signals and extract time and amplitude information. In order to do that we use a digital implementation of a constant fraction discriminator which provides timing for a fixed pulse shape independent from the pulse amplitude (Fig. 4.3). It works classically in the following way: the incoming signal is split up into two pulses where one of them (1) is inverted and delayed while the other one (2) is attenuated to a certain fixed fraction of the incoming signal. The sum of both pulses becomes zero at a time independent of the pulse amplitude. Using a digital implementation of the algorithm one has to optimize the parameters in a way that the algorithm is precise on the one hand and efficient on the other hand. Digitalization with a certain sampling rate allows only to delay signal (1) by a multiple of clock cycles while efficiency suggests not to attenuate signal (2) what would need a division but to amplify signal (1). The timing is calculated via the difference of the delayed and amplified signal from the original one, adding a constant offset to avoid negative values, where the point of zero crossing now is the point reaching this offset. Because of the discrete time structure of the samples in multiple of clock cycles (12.86 ns) the value obtained by this method has only a precision of one clock cycle. In order to get a more precise timing a linear interpolation between the samples before and after the zero crossing is applied. Therefor the amplitude of the difference before (a) and after (b) the point of zero crossing are subtracted from each other and (a) divided by this value:

(4.1)
$$t = \frac{a}{a - b}$$

To avoid the time consuming division a lookup table (LUT) for $1/(a-b)$ is used which has a 6 bit wide input and a 7 bit wide output. In order to fit the signal into this LUT and to get a consistent result the values of (a) and (a-b) were reduced to span the width of the 6 most significant bits of (a-b) starting from the first bit being not zero ($\mathrm{max_{nz}}$). The time value calculated by this is 13 bit wide and described by

(4.2) $\quad \mathrm{t(12\ downto\ 0) = a} \left[\mathrm{max_{nz}\ downto\ (max_{nz}} - 5) \right] \cdot \mathrm{LUT} \left(\mathrm{(a\text{-}b)} \left[\mathrm{max_{nz}\ downto\ (max_{nz}} - 5) \right] \right).$

The values in the LUT are shown in appendix A.1.

4.3 Energy Summation

The energy value is calculated from the maximum amplitude value after the CFD hit. In order to get the maximum of the pulse it is determined by comparing three neighboring samples starting at a certain sample around the CFD transition. This value is multiplied with a calibration constant and then all those energy values within one MSADC, which were selected, are added. In further steps the energy values from all MSADCs are first summed up between each other on the carrier cards and then on the backplane (Fig. 4.4).
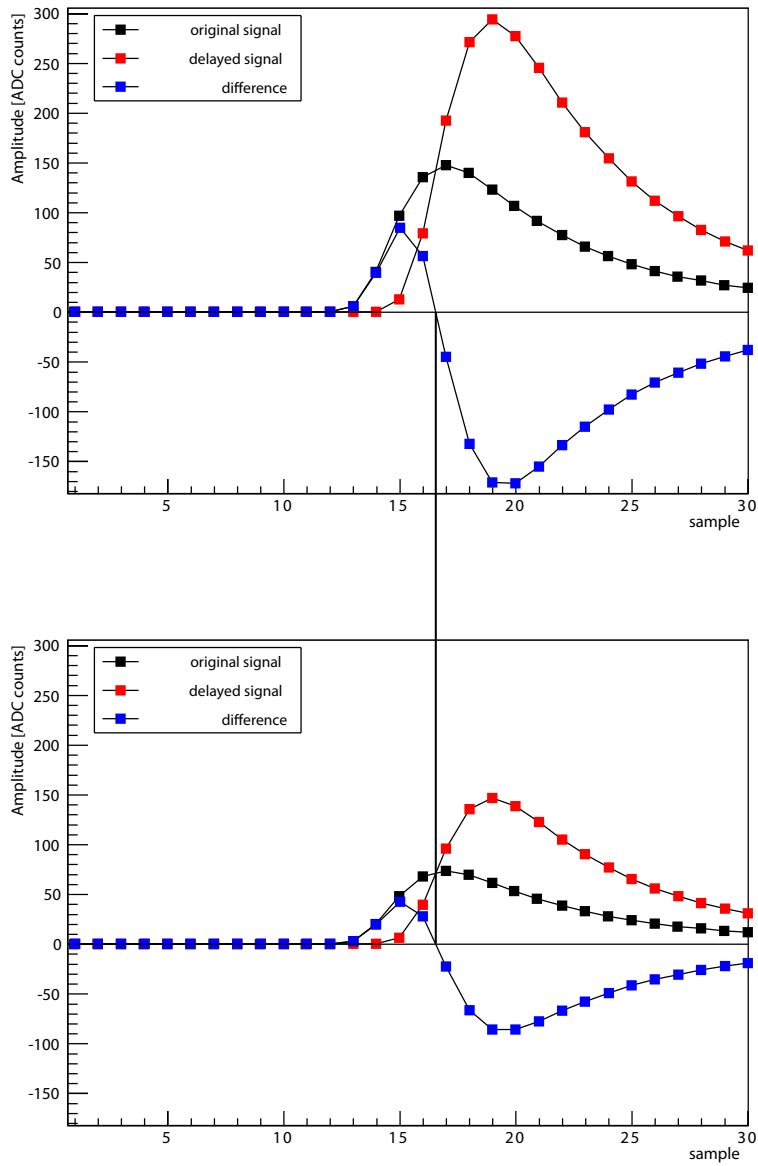
Figure 4.3: Digital constant fraction discriminator for two signals with different amplitudes. The curve with the black markers is the original signal coming from the ADC. The curve with red markers is the signal delayed by two clock cycles. The blue one shows the difference between the two signals. The vertical black line connects the points of zero crossing.
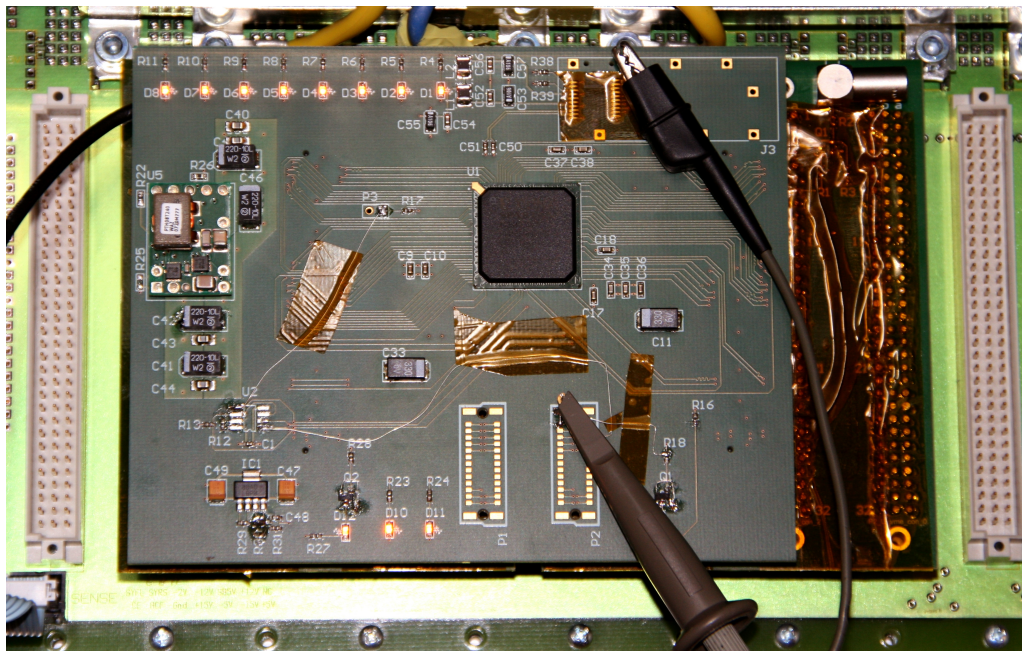
Figure 4.4: Photo of the prototype VME backplane used in 2009.

4.4 Time Adjustment

The time extracted as described in section 4.2 has to be corrected for constant offsets between the channels which are caused e.g. by different cable lengths. This values are calculated offline using the COMPASS online filter Cinderella. This time correction values are stored in a database from where it is read and loaded into configuration registers of the FPGAs. The coarse times, i.e. timing values in multiples of clock cycles of 12.86 ns, are directly used to adjust the depth of delay buffers in the FPGAs. In addition the fine time, i.e. remaining parts smaller than 12.86 ns are added to the time calculated in the FPGAs. Using this fine time information the signal is delayed once more if the timing exceeds the length of one clock cycle. For smaller values the most significant bit is used to determine, if the signal appeared in the first or the second half of one 12.86 ns second period. Depending on this value the width of the energy information is extended in positive or negative direction respectively (Fig. 4.5). This method of using time bins allows to always have the energy of one physical signal in the same time bin and so being able to calculate the energy sum for one physical event.

4.5 Theoretical Energy Resolution

The 12 bit wide data coming from the ADC is multiplied by the 10 bit wide energy calibration coefficient. This increases the data size to 22 bit. In order to pass this data through the interfaces connecting the different FPGAs, the data size has to be decreased. The first
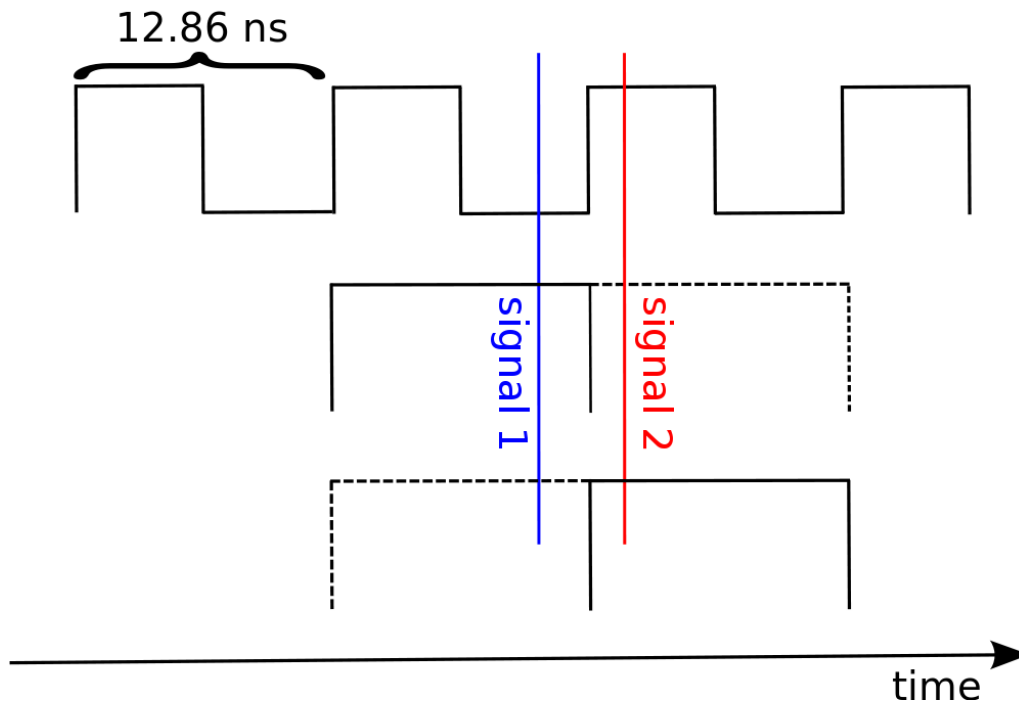
Figure 4.5: Method of time adjustment. If the fine time is bigger than 6.43 ns, the signal is extended into positive direction, otherwise into the negative one.

selection is done directly after applying the energy calibration where the 22 bit wide energy is decreased to a 12 bit wide value by selecting the 12 most significant bits (MSB). After this the data of all 16 channels in one mezzanine card are summed up to form a new 16 bit wide sum value. Knowing that the maximum physical relevant energy is the same as the maximum of one individual channel, the size can be decreased to 12 bit by selecting the least significant bits (LSB) and setting values bigger than the maximum value of 0xFFF to exactly this value. As this interface is set to a frequency of 160 MHz and having 6 parallel data lines, this 12 bit value can be transmitted to the carrier card. On the carrier card again a summation of 4 mezzanine cards is performed, where the data size again increases to 15 bit selecting the 9 LSB as before. This data can be transmitted to the backplane. Calculating all this steps for an example energy of 15 GeV, deposited in a single channel, with an energy calibration constant of 41.25 MeV/(ADC channel) loaded as a calibration coefficient of 412 to the FPGA one gets a theoretical energy resolution of approximately 0.83 GeV for the final sum value.

4.6   Trigger Decision

The trigger decision is made at the stage of the final energy summation. This value is compared with a chosen threshold and sets a trigger bit to one as long as the sum is above

threshold. The binary value is connected to the output of the backplane FPGA which is accessible via a LEMO connector. The connector is than connected to a coaxial cable which transmits the information to the analogue trigger system. There a coincidence is made with the beam trigger, which has to be timed in respectively to the ECAL signal. This provides the final trigger information for the readout system. The trigger time is made from the TDC information of the rising edge of the coincidence.

4.7 Interfaces

Due to the huge number of channels in ECAL2 the trigger logic is spread over several FPGAs. If the clock on the receiver side is not synchronous with the data, the data gets corrupted in a way that single bits are read at a wrong time. In order to fix that the data quality can be checked by generating a certain pattern on both sides of the interface and comparing the results. In our case we use a pseudo random generator consisting of a shift register where bit zero is set to the XOR of the two most significant bits. By doing so all bit combinations, except of the zero combination, are generated in a way that the values differ in quite many bits from clock cycle to clock cycle (Table 4.1) . If due to an error the zero combination is reached, the system starts again with another fixed pattern.

In order to check the interface the receiver side generates the next pseudo random value from the previous received value. That allows that the generator never goes into an idle state. If the values calculated on the received value do not match with the generated one an error counter is incremented. The clock phase on both sides is adjusted as long as the error counter is not equal to zero what can be checked via LEDs as well as read via the I^{2}C interface.

Different latencies for different ADC cards are adjusted by sending a fixed pattern several clock cycles after the reset. The backplane waits until this pattern is received and delays the signals which come earlier by the difference in clock cycles to the latest one.

For the 2009 run this values were tested in the beginning and assumed to be stable. In order to have control over this settings and to be safe that no errors occur, a monitoring system should be implemented for the future.

It	Value	Binary	It	Value	Binary	It	Value	Binary	It	Value	Binary
0	1	000001	16	19	010011	32	9	001001	48	13	001101
1	2	000010	17	39	100111	33	18	010010	49	26	011010
2	4	000100	18	15	001111	34	37	100101	50	53	110101
3	8	001000	19	30	011110	35	11	001011	51	42	101010
4	16	010000	20	61	111101	36	22	010110	52	21	010101
5	33	100001	21	58	111010	37	45	101101	53	43	101011
6	3	000011	22	52	110100	38	27	011011	54	23	010111
7	6	000110	23	40	101000	39	55	110111	55	47	101111
8	12	001100	24	17	010001	40	46	101110	56	31	011111
9	24	011000	25	35	100011	41	29	011101	57	63	111111
10	49	110001	26	7	000111	42	59	111011	58	62	111110
11	34	100010	27	14	001110	43	54	110110	59	60	111100
12	5	000101	28	28	011100	44	44	101100	60	56	111000
13	10	001010	29	57	111001	45	25	011001	61	48	110000
14	20	010100	30	50	110010	46	51	110011	62	32	100000
15	41	101001	31	36	100100	47	38	100110	63	1	000001

Table 4.1: Results of the pseudo random generator in a 6 bit version. The column named It gives the number of the iteration, Value describes the value calculated with the pseudo random algorithm and Binary is the value shown in binary format. As one can see all numbers from 1 to 63 are present and in the 64 iteration the initial value is reached.
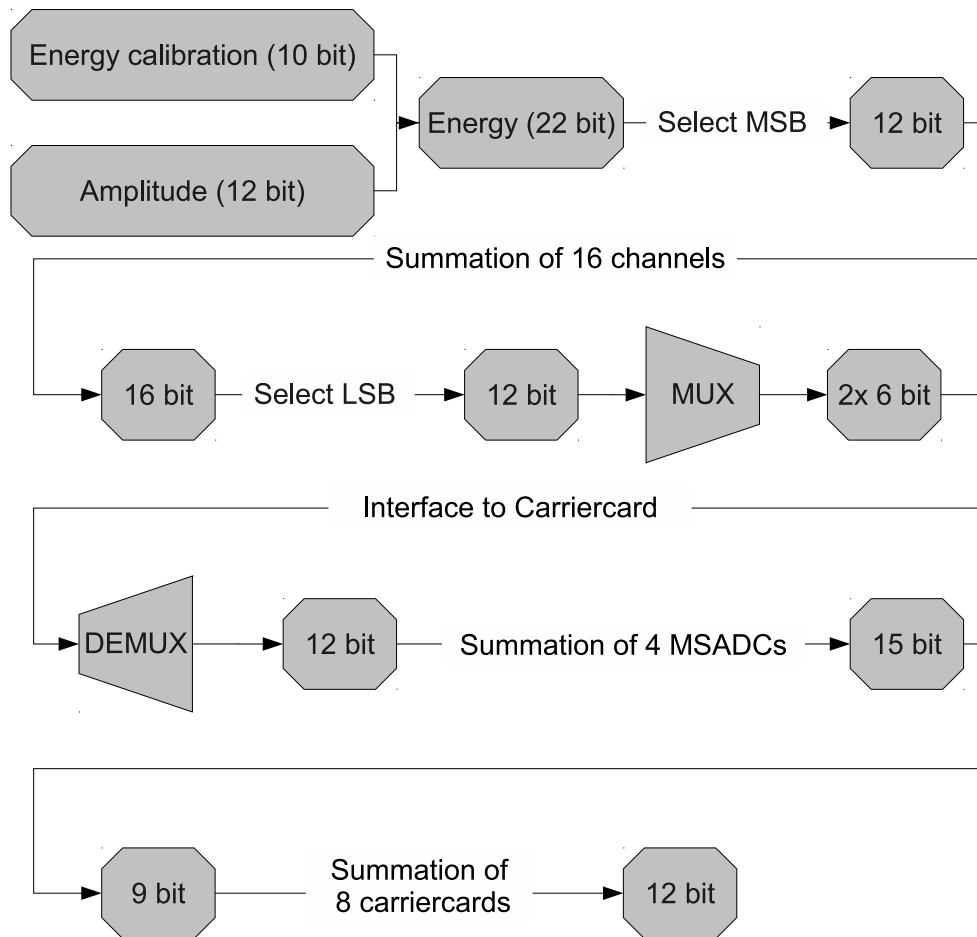
Figure 4.6: Flow of the size of the amplitude value for one channel. The increase by multiplying with energy calibration constant as well as due to the summation with other channels is shown. The decrease of width is done to be able to pass through the interfaces between the different FPGAs

Chapter 5

Performance of the Digital Trigger

In order to study the physics obtained from the data taken with the electromagnetic calorimeter, its performance during data taking has to be studied very precise. In order to do that a combination of simulations of the trigger using analysis tools on physics data as well as online monitoring of values calculated within the FPGA have to be used. Further parameters of the interfaces should contentiously be monitored to be sure that all data runs synchronously.

5.1   The 2009 Trigger Settings

During the Primakoff run in November 2009 the first test of the trigger system was performed. The usage of one single backplane summation card allowed to connect eight carrier cards with a total amount of 512 detector channels. These channels had to be arranged in a rectangle with an area of 16 columns times 32 rows. In order to have a total trigger rate around 30 kHz an area of 12×12 channels around the neutral center was selected with 3×4 channels excluded around the beam hole. The trigger thresholds were set to 60 GeV and 40 GeV. The 40 GeV threshold was prescaled with a factor of 2. This resulted in trigger rates of 20 kHz for the lower threshold and 23 kHz for the higher one and due to the biasing of the two thresholds to a total rate of 26 kHz. All these values were obtained while running at a beam rate of 2.5 MHz. An occupancy plot with the trigger area shown can be seen in Fig. 5.1.

5.2   Baseline Stability

It was foreseen to read out the individual baseline values for every channel and for every spill. Unfortunately the readout via I^2C during data taking did not work as expected. This values would give information about the long term stability of the baseline as well as about the error in determining it. The value one can determine without this information
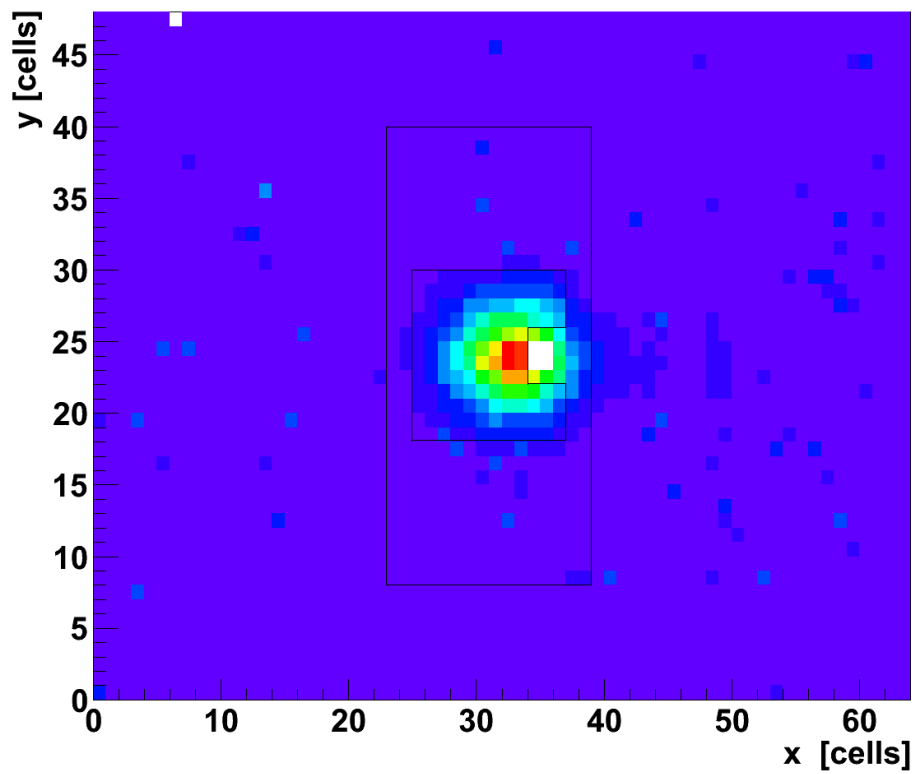
Figure 5.1: Occupancy of ECAL2 during the Primakoff data taking. The area selected for triggering is shown within the black lines in the center. The additional rectangle shown is the area which would have been possible due to geometrical reasons.

is the baseline value calculated from the first view samples of the LED calibration data, where in contrast to physics data pile up is not present (Fig. 5.2 a). The data clearly shows that the baseline is very good centered around a value of 50 ADC channels. A fit with two Gaussian curves results in a width of around two ADC counts where the mean value of the second Gaussian is a bit higher than 50. Looking at data taken with the test beam this second part disappears. That means it is a noise contribution resulting from the setup at compass with many channels. In figuref 5.2.b) the baseline measured at the testbeam is shown. There the smaller calorimeter was less noise and thus the width of the paseline distribution is a clear measurement for the accuracy of the measured value.

5.3   Per Channel Hit Rates

Via the I^{2}C interface also a monitoring of the hit rates of the CFD per channel were foreseen. This would allow to have better control over the per channel threshold and the associated treatment of noise. Increasing hit rates would give a hint to noise cells in the calorimeter as well as zero hit rates correspond to dead cells.

5.4   Time Resolution

A very important quantity is the time resolution of the constant fraction discriminator. In Fig. 5.3 the integral time resolution of the CFD is shown calculating the fine time directly without using the lookup table. As one can see the time distribution can be described as a sum of two Gaussians plus a constant background. Resulting from this the average σ can be calculated via

(5.1) $$\sigma = \frac{\sigma_0 \cdot \mathrm{const}_0 + \sigma_1 \cdot \mathrm{const}_1}{\mathrm{const}_0 + \mathrm{const}_1}.$$

This gives a result of $\sigma =$1.04 ns. This global result can be split up in a part coming from the used algorithm and a part coming from contributions of the signal shape and noise.

To distinguish this timing analysis as a function of the amplitude is useful. Therefor the time is plotted as a function of the amplitude in Fig. 5.4. One can clearly see that the width of the peak decreases quite fast with increasing amplitude while some background is present for all energies resulting from pile up. There is also a more prominent component and very low energies coming from noise. Qualitatively this plot already shows the effect quite well but can be misleading due to the bigger statistics at lower amplitudes.

In order to get a real impression the width of the time residual was determined as a function of the amplitude taking into account all entries within 10 ADC channel bins. The result is shown in Fig. 5.5. There the width is plotted as a function of amplitude and fitted with an exponential plus a linear polynomial. While the exponential is describing the resolution for low amplitudes, the polynomial is the function describing the width
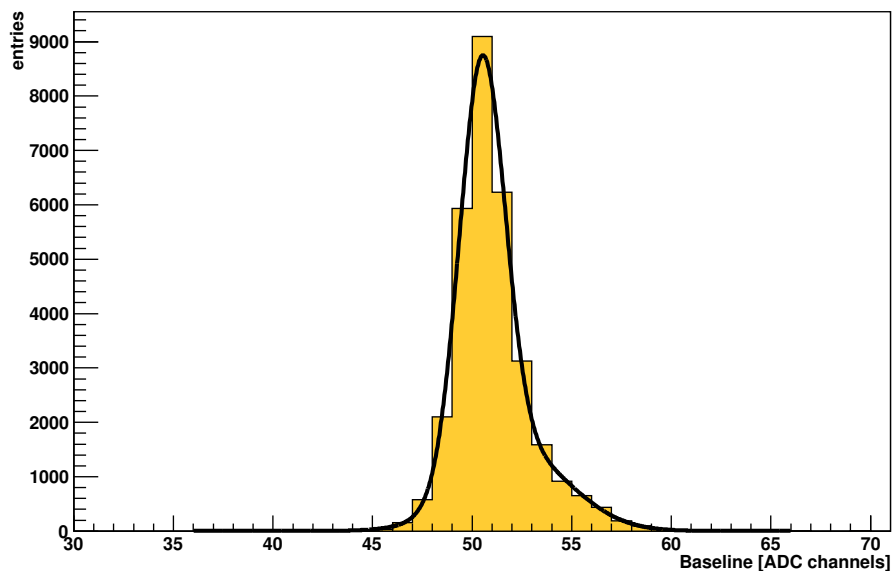
(a)
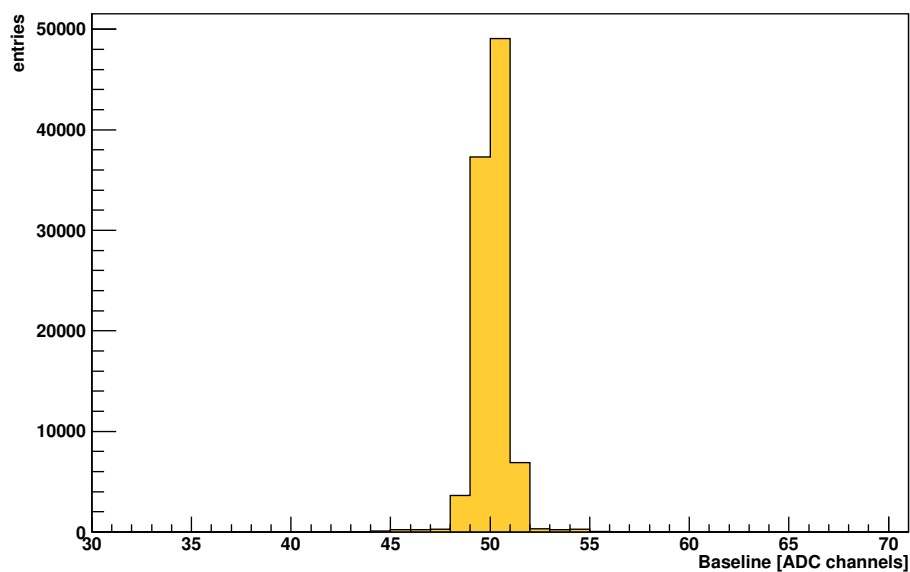
(b)

Figure 5.2: Pedestal distribution a) Measured with calibration signals at COMPASS b) Measured at the testbeam setup
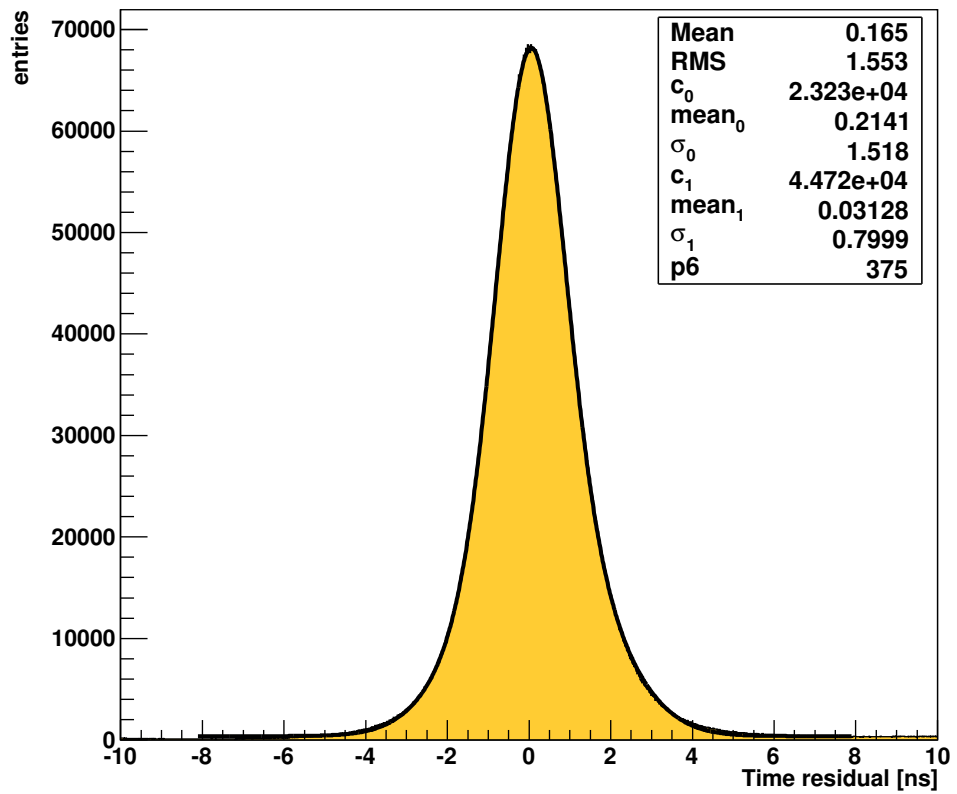
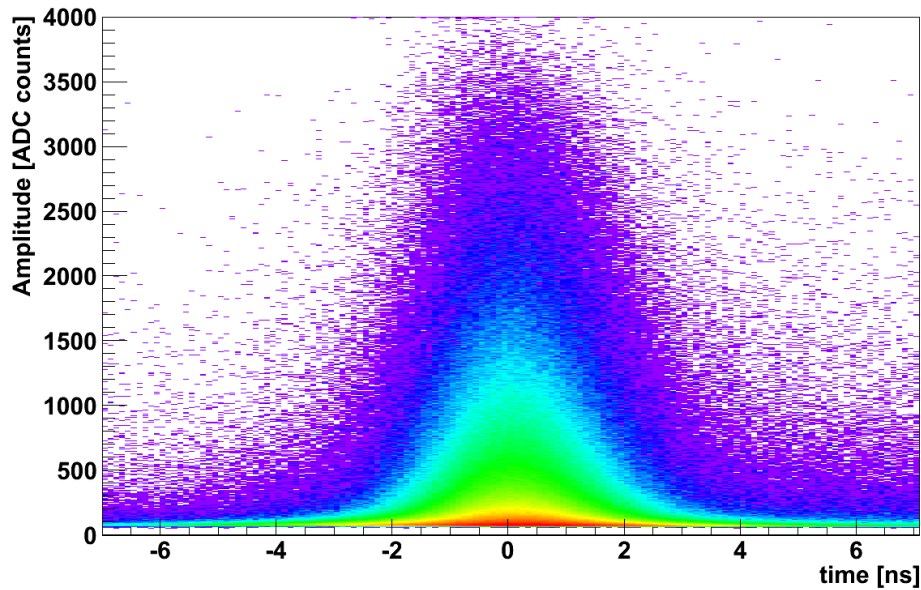**Figure 5.3:** Integral time resolution plot. Fitted with two Gaussians and a constant background.

Figure 5.4: Time resolution of the CFD as a function of the amplitude.

above approximately 200 ADC channels. Looking again at the distribution of the baseline (Fig. 5.2) which reaches up to 60 ADC counts, it comes out, that noise is only contributing to the resolution at low energies and has for instance an effect up to 10% at amplitudes of around 100 ADC channels. This is also the deviation from the polynomial one can observe in Fig. 5.5. That means the function

$$(5.2) \qquad\qquad \sigma(x) = A \cdot \exp\left(-\lambda \cdot x\right) + m \cdot x + t$$

can be seen as a combination of to independent contributions where the exponential describes effects coming from the signal, while the linear polynomial describes the quality of the algorithm as a function of the amplitude. The slightly decreasing width in this case could be attributed to a smaller impact of the limited sampling resolution of 12 bit as well as to a increasing linearity in the rising edge of the pulse.

It depends on the precision of the timing coefficients loaded into the FPGA, the noise while determining the spill based baseline and the noise on the physics pulse. Further the quality of the LUT, which is used for division, and the bit precision of the values we use for calculating the time have some impact.

The study of this quantities can be very efficiently done offline. For the study of the LUT a small program has been written, taking into account all possible combinations of $\frac{a}{a+b}$ in the range of $0 < (a+b) < 4000$ and $a < (a+b)$. The result can be seen in fig. 5.6. In the left image the dependence of the time residual on the calculated time can be seen. It is clearly visible, that the energy resolution becomes worse for bigger times. This comes from the non linearity of the decision. That means that for small times the quotient is
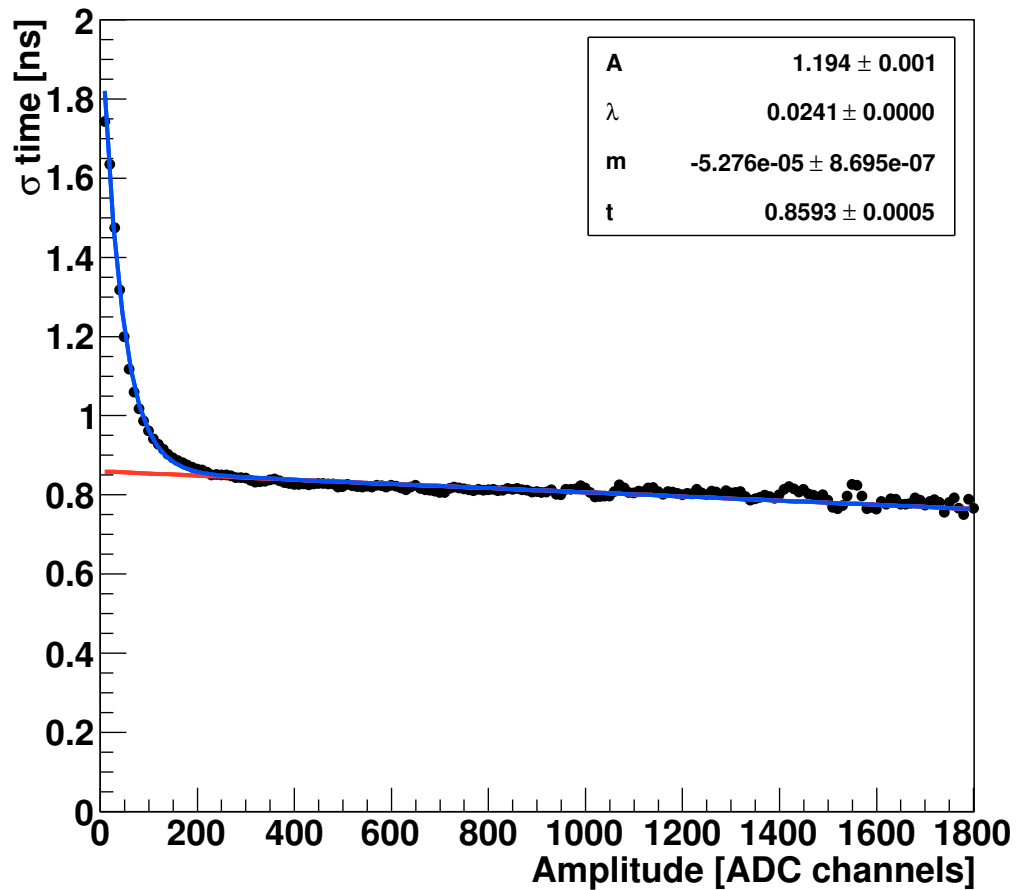
Figure 5.5: Width of the timing peak for certain amplitudes. Fitted with an exponential plus a polynomial: $\sigma(x) = A \cdot \exp(-\lambda \cdot x) + m \cdot x + t$ (blue curve). The polynomial (red curve) corresponds to the time resolution coming from the pure amplitude dependences of the algorithm. The exponential comes from the influences of noise to the result.

determined by the most significant bits, while for high times the quotient is determined more and more by the less significant bits, which are cut away to reduce the size of the LUT. In the middle picture of figure 5.6 the total residual of the time is shown. What is conspicuous is, that the time calculated using the LUT has an offset of approximately 200 ps to smaller values than the exact determination of that quantity. In the right picture the dependence of the residual on the amplitude is shown. The rectangular shapes are representing areas in which the same bits are selected to calculate the time. One can see that the residual increases for higher amplitudes because the number of significant bits, which are not used in the calculation, also increases.

(a)

(b)

(c)

(d)
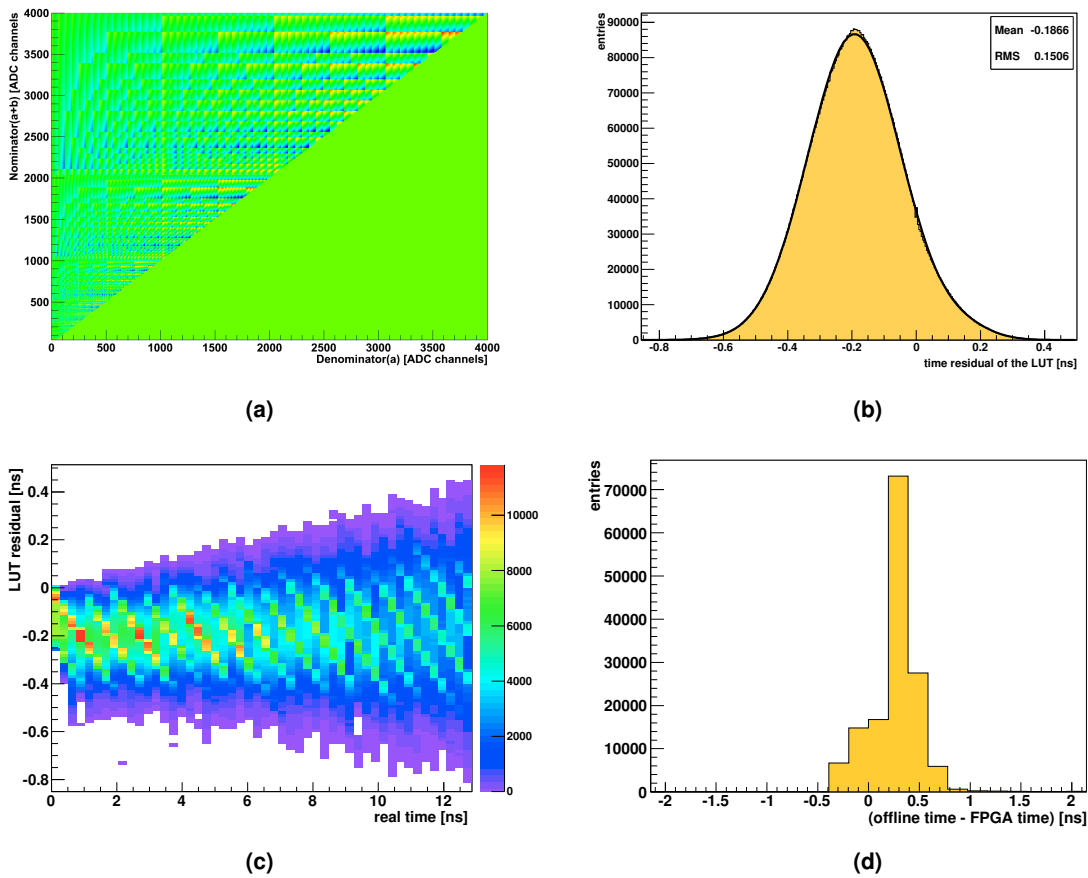
Figure 5.6: Time resolution. (a) shows the dependence of the signal amplitude. In (b) the time residual is shown. In (c) the time residual is shown as a function of time. In (c) the measured time difference between FPGA time and offline time from the test beam is shown. The average amplitude here is 1200 ADC counts.

5.5   Problems During the 2009 Run

5.5.1   Determination of the Wrong Amplitude

As explained in section 4.3 the amplitude is determined by a scan over a certain number of samples. The position of this samples was determined in advance. In the analysis it turned out that the scan was not performed in an optimal way. This problem can be seen in figure 5.7 where the amplitude determined by offline calculation of the maximum value of all 32 samples is shown as a function of the value returned by the FPGA. Therefore cuts were taken to have exactly one CFD hit in the samples to ensure that the maximum corresponds to the value calculated by the CFD. The few bigger deviations at low amplitudes come from events occurring right at the end of the sample window. To estimate the effect on the amplitude resolution an upper limit for the fraction of FPGA amplitude and offline amplitude was found to be 14% for amplitudes above 200 ADC counts. For lower amplitudes the quality of the CFD result is worse (fig. 5.5) and thus the relative effect of the amplitude error increases while in addition also noise contributions have a bigger influence on the residual value .
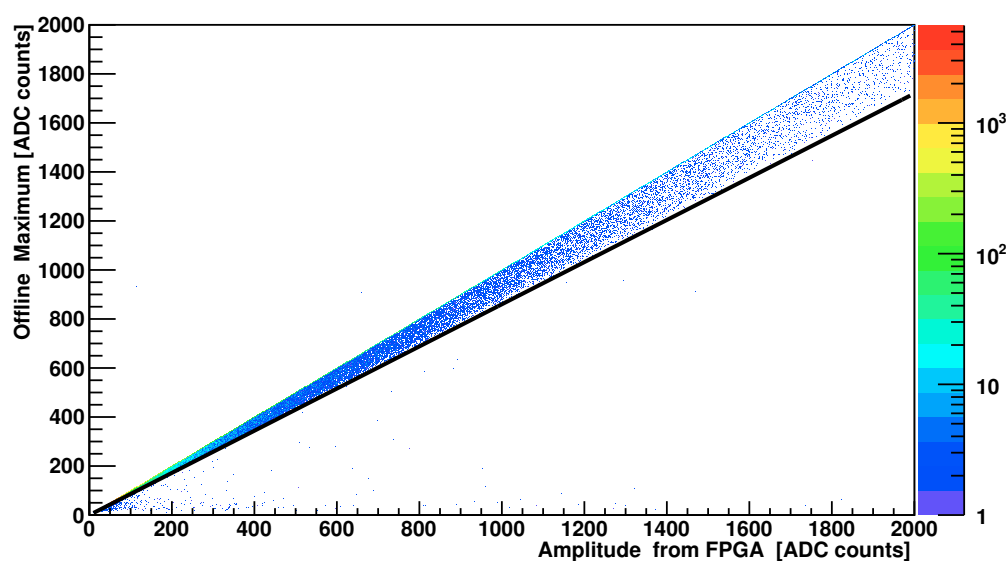
Figure 5.7: Amplitude determined by offline calculating the maximum of all 32 samples versus the amplitude returned by the FPGA. The scattering of the FPGA amplitudes is limited by a straight line with a gradient of 0.86. This corresponds to the maximal difference to the sample close to the maximal one.

The 14% are resulting from the pulse shape and they are the maximum deviation a sample, which is taken from the upper part of the rising edge, can have respectively to the real maximum. The studies concerning this problem were done excluding cells affected by the timing problem described in section 5.5.2. This leads to many entries in the histograms at low energies which can be ignored for this analysis.

The effective impact on the trigger is shown in figure 5.9. The resolution determined by fitting a Fermi function (not shown) to both curves gives a width of the rising edge of $\Delta E = 1.5$ GeV for the curve when having a mismatch in the amplitude, while the correct amplitude has a width of $\Delta E = 0.7$ GeV.
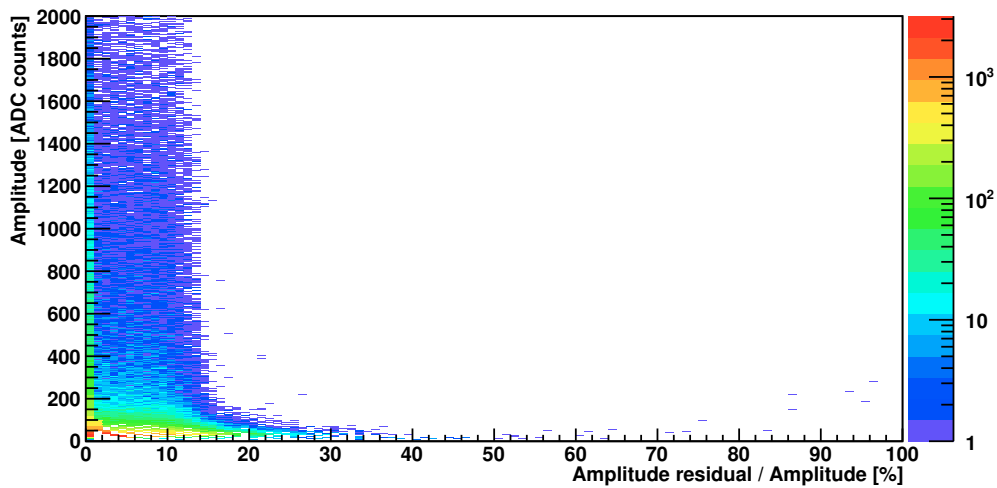

Figure 5.8: Amplitude as a function of the relative amplitude residual being $\frac{\text{Amp}_{\text{offl.}} - \text{Amp}_{\text{FPGA}}}{\text{Amp}_{\text{offl.}*100}}$. Clearly visible is the boundary at around 14%.
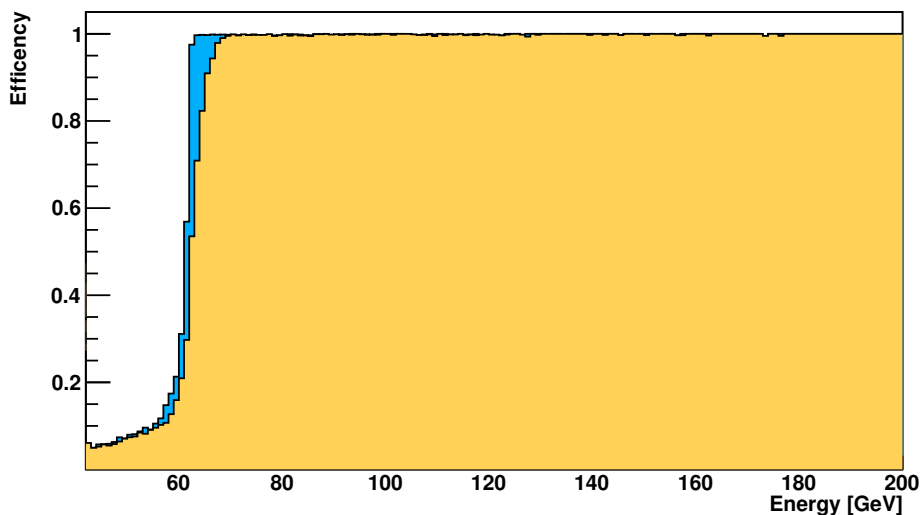
Figure 5.9: Efficiency plot of the 60 GeV trigger dependent of the method of amplitude selection. In yellow the correct amplitude is calculated offline. In blue the same amplitude is taken like in the FPGA. This visualizes the loss in resolution obtained due to the wrong selection used.

5.5.2 Time Jumps at the ADC Interface

The worse problem was that the time synchronization to the ADCs did not work reliably. Becauseone ADC is connected to eight detector channels the time jumps always occur on all eight channels simultaneously. The sets of eight channels are called channel groups from now on. The jumps were caused on the one hand by procedures to decrease the latency needed during the synchronization in order to match the timing requirements of the analogue trigger on the other hand the additional logic used within the FPGA increased the power consumption and with it the thermal output. This shifted the clock relatively to the clock sent to the ADC and thus the synchronization was not stable anymore. A FIFO used in between avoided corruption of the data. The timing issue was not preserved, because the status signals, which have to be transmitted between the two clock domains were asynchronous. . The problem is that the empty signal runs synchronously with the clock used for writing, while the read enable signal runs with the clock for reading. In case the two clock phases are at a boundary the read enable signal is issued either a clock cycle earlier or later. This is illustrated in figure 5.10. The official statement of XILINX is:

> "If the rising WRCLK edge is close to the rising RDCLK edge , EMPTY could be deasserted one RDCLK period later." [7]
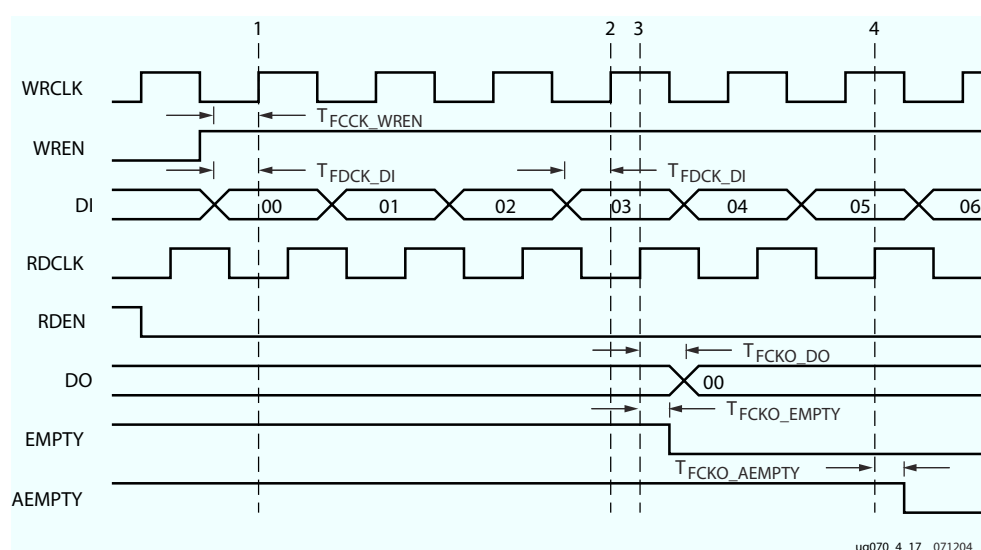

Figure 5.10: Timing diagram of a FIFO implemented in the XILINX Virtex4. Illustrating the dependence of the status flags on the read and write clock. A wrong phase relation of these two clocks can cause a glitch in the empty signal. Taken from [7].

If the clock phase is at such a boundary condition it depends on the run time between FPGA and ADC. This is influenced as well by the impedance on the connection as by the temperature. Both parameters are not absolute identical for all of the MSADC cards forcing them to be influenced differently. In figure 5.11 a) is shown how often the individual

channel groups are affected by the glitches. The total number of channel groups is 384 of which around 20 (5%) are affected in 50% of the spills or more. A distribution of the number of channels affected is shown in figure 5.11 b).
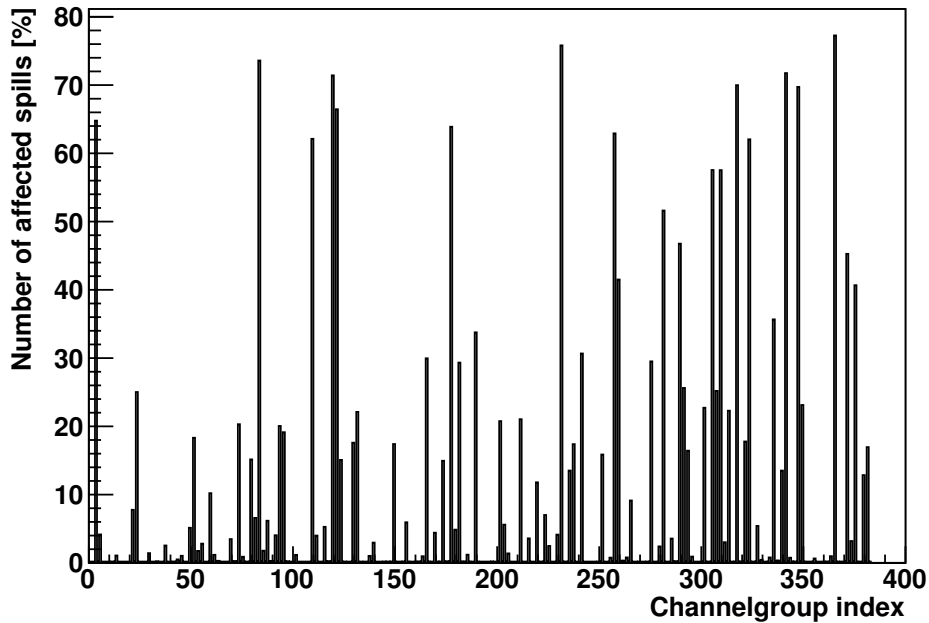
(a)
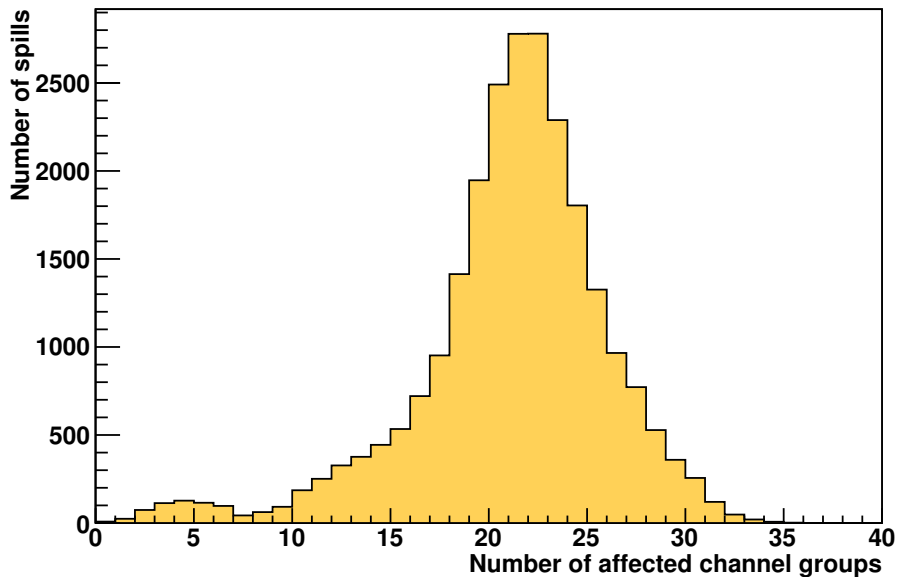
(b)

Figure 5.11: a)Occurrence of the glitches in the different channel groups. b)Occurrence of the glitches in the different channel groups.

5.5.3 Effect of the Time Jumps on the Trigger

The impact on the trigger is quite complex due to the fact that the trigger does not cut on a certain signal time but uses the binned method. In that way the pulses being shifted by one clock cycle of 12.86 ns are still overlapping in most of the cases with pulses which have the correct time. The trigger is affected in case the time is determined wrongly for signals for which then the bins are extended in the wrong direction and thus the overlapping is not ensured anymore. In the other case the trigger is influenced when the analogue beam trigger signal is not in coincidence with the overlapping signal providing the correct energy.
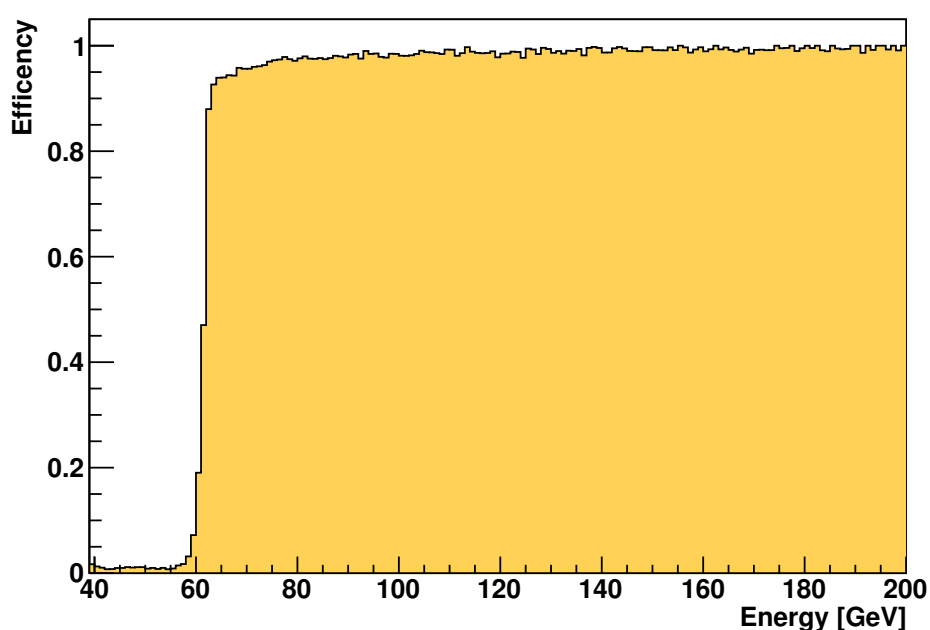
Figure 5.12: Amplitude as a function of the relative amplitude residual being $\frac{\text{Amp}_{\text{offl.}} - \text{Amp}_{\text{FPGA}}}{\text{Amp}_{\text{offl.}*100}}$. Clearly visible is the boundary at around 14%.

The time dependence can be visualized by using the time calculated within the calorimeter (Fig. 5.13 a) as well as the TCS phase (Fig. 5.13 b), which in principle provide redundant information. To produce these figures both times were calculated under the condition that the energy of the time corrected signal exceeds the threshold of the trigger with the higher threshold (60 GeV) while only the low threshold trigger gave a signal in the experiment. By doing so only events having problems with the time jump are selected. In both figures a double structure can be seen corresponding to two clock phases of the MSADC system fitting into one TCS clock phase. The additional smaller peak is due to the fact that the rising edges of the two clocks are not matched at the place where the trigger decision is made. This third peak corresponds to one of the other two if one subtracts 25.72 ns from its time value. That means a possible solution to get a data set for

analysis, which is less affected by the timing problems, is to apply time cuts on the TCS phase selecting only events which lie next to a TCS phase of 45 ns and 57 ns. This solution does not seem to be usable because the timing values of events triggered by affected cells are due to the time jump biased to TCS phases around 48.7 ns and 61.4 ns (Fig. 5.15) which would be cut away be see selection mentioned above. This would lead to a nearly complete exclusion of events in these detector cells.

The best way to perform a real clean data analysis is to select spills in which the trigger area was not affected by the time jumps. This is possible for 32% of all spills due to the fact that out of the 24 channel groups which are contributing to that area only three have a significant probability for glitches (Fig. 5.14 a). In total it turns out that 32% of all spills taken where not affected (Fig. 5.14 b). This makes a total amount of 3216 recorded good spills for analysis.

An additional effect of this circumstance is that the trigger time stored in the TCS phase has two peaks with a distance of one clock cycle. This peaks occur when a pulse related to a shifted cell contributes to the energy sum activating the trigger and rising edge of the ECAL2 trigger gets in coincidence with the beam trigger signal. In this case the time is not given by the rising edge of the beam trigger but by the calorimetric trigger which is synchronous to the 12.86 ns clock. The effect is shown in figure 5.15. There the TCS phase is plotted as a blue histogram with an event selection for events with an energy deposition in the trigger area above 80 GeV applied. The peaks are present and dominating in the green curve where a cut is applied excluding events, which are above 80 GeV even without cells, which were shifted in time. The yellow curve which is the difference of these two curves clearly has the peaks removed. That shows that the interpretation is correct. The plot of the TCS phase distribution is implemented in the COOOL monitoring program of COMPASS but it is not a part of the bookies controlled every shift. Checking it during the run would directly have given a hint that there is a timing problem.

5.6   Handling the Time Jumps in Offline Analysis

Because the time jumps occur on the interface to the ADCs all data coming from the detector is affected by the jumps. That means also the timing for the data used in analysis has to be corrected in order to produce correct clusters in the detector. For that purpose for each run a file was produced containing time correction values for each spill of the run. This was done using a newly developed preprocessing class in the data reconstruction framework CORAL (COMPASS reconstruction and analysis library). There a reference time is read in and subtracted from the event time. This data is filled into 5 bins per channel group from which the bin with the maximum entries corresponds to the offset, which has to be applied (bin 2 corresponds to no offset). The resulting bins are stored into binary files with a header containing checksums for every spill for data integrity checks. This preproduction procedure has been made for all physics runs after
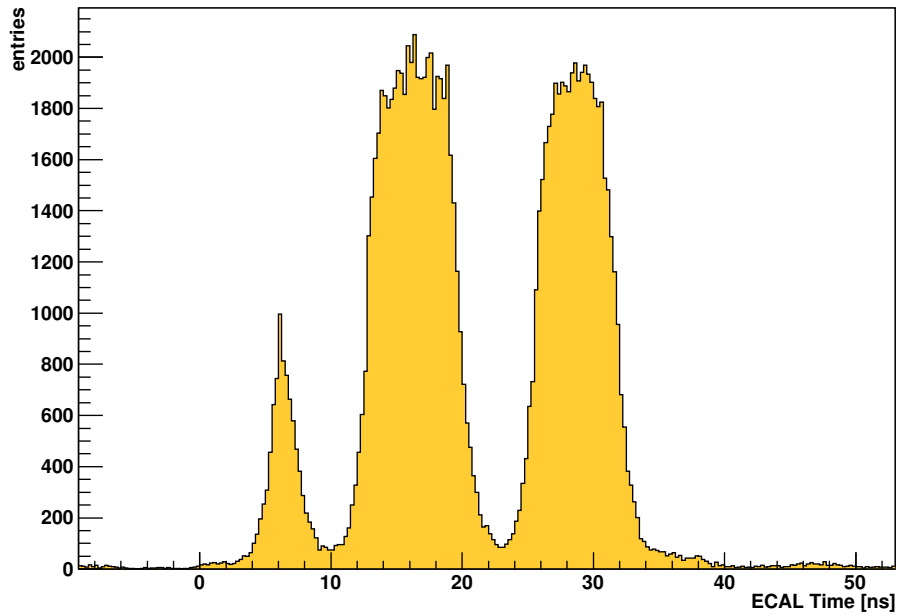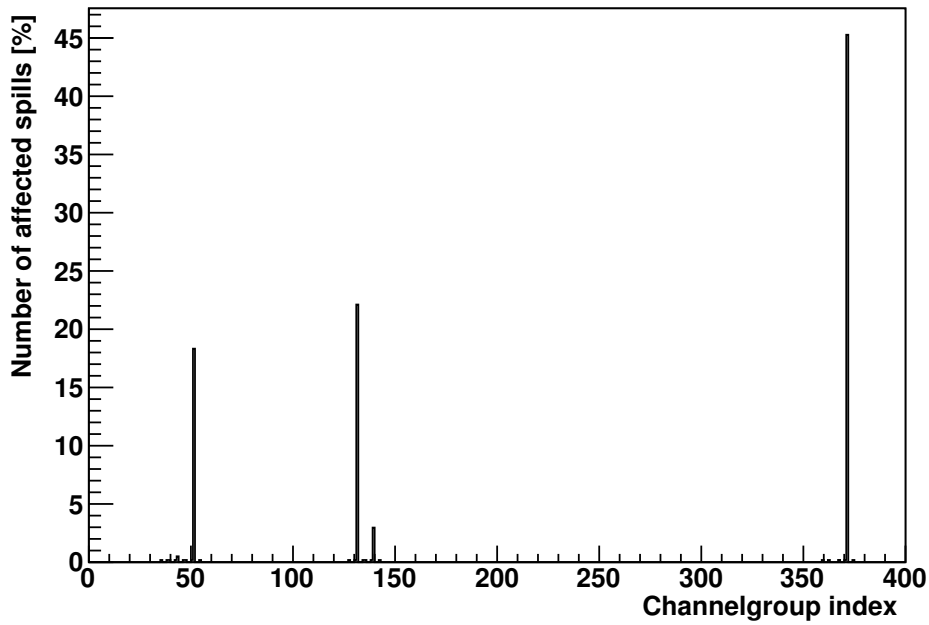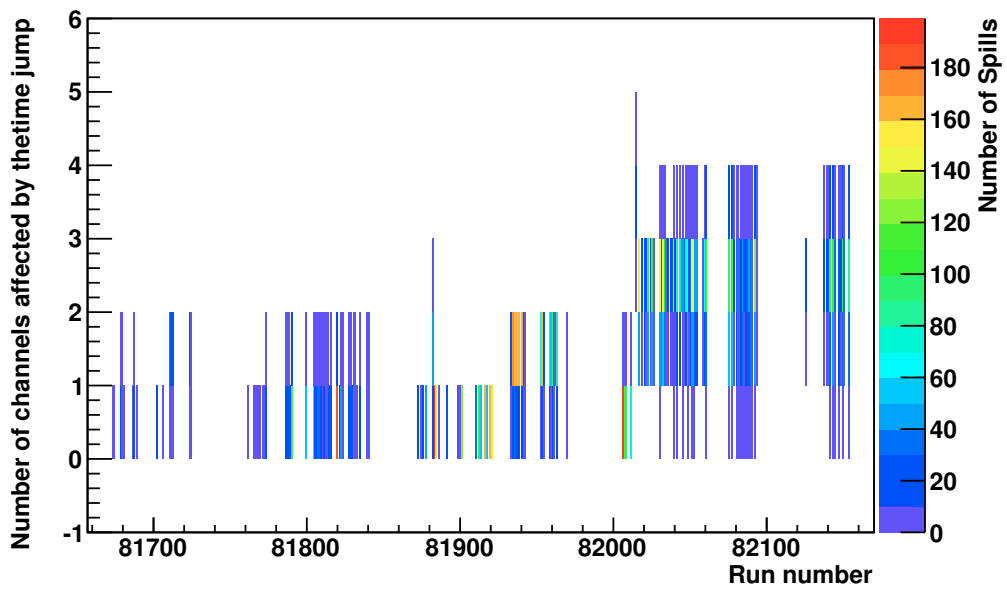
(a)
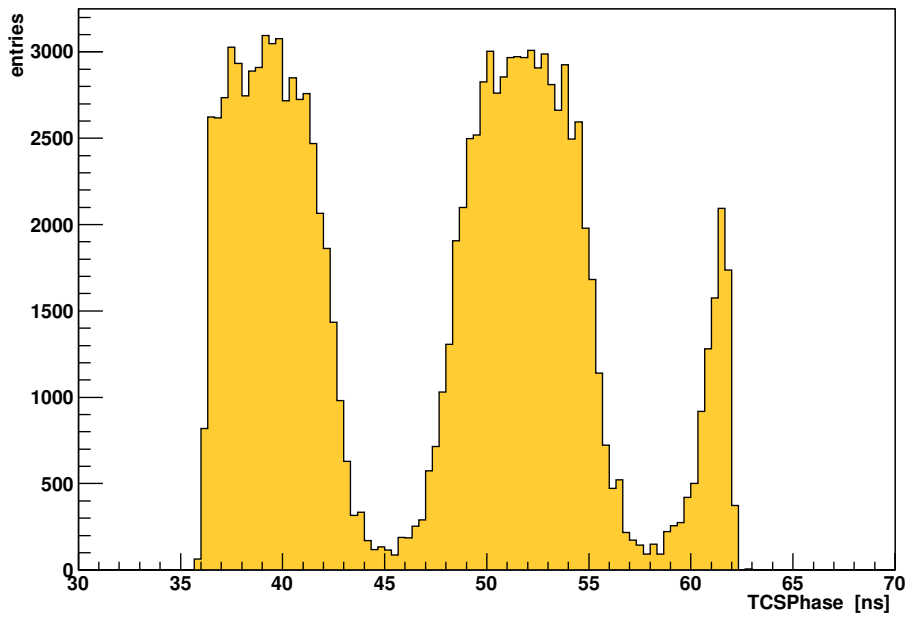
(b)

Figure 5.13: Time distribution of events for which the trigger is affected by the time jumps. Spectra show the times where the energy sum is above a certain threshold when the time is correct but which are below that threshold with a time shift. In a) the distribution of the time as seen in the calorimeter is shown. In b) the distribution of the TCS phase.

(a)

(b)

Figure 5.14: a) Distribution of the probability that a certain channel group has a glitch within a spill. Only channels in the trigger area are shown. b) Distribution of the number of channel groups in the trigger area, that were affected by the glitches for each run. The color coding gives the number of spills per run.
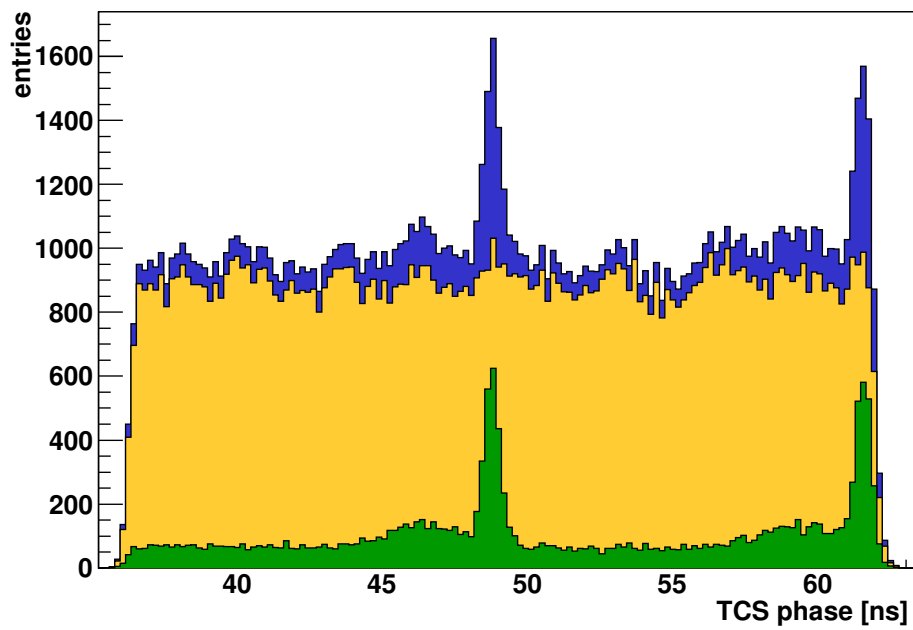
Figure 5.15: The TCS phase distribution for events with an energy deposition above 80 GeV is shown in the blue histogram. Clearly visible are spikes at 48.7 ns and 61.4 ns. These come from contributing cells which are shifted in time (green histogram). A flat TCS phase is recovered for the remaining events where the shifted cells did not contribute to the trigger (yellow histogram).

a certain point in time from which on it turned out that the problems were present. The produced files are on read back by CORAL during the real data processing and the the timing values corrected by them. The data used for physics analysis are not affected by timing errors anymore and no one using them has to take care about it.

5.7   Necessary Improvements

As seen from the data there are some improvements that have to be done. The time jumps, also affecting the readout, have to be fixed. This was already done in April 2010 in order to avoid affecting the data taking in 2010. Further the amplitude determination has to be improved to really fetch the maximum sample. Further the monitoring has to be improved. For reading out the registers for scalers and baselines, I^2C was not working well. In order to get this done, it is foreseen to store this information in the data stream from the mezzanine card. This data then will be identified by the GeSiCA and filtered out into registers on that module. These can be read out via VME registers and therefor disturbing of and from the readout will be avoided.

Further also the stability of the timing should be monitored online. For the timing of the individual channels several ways are possible and should be considered in parallel. The most direct way is to simply calculate the timing from physics pulses and compare it to a reference value in a similar way as it was done during the preproduction of 2009 data (section 5.6). This approach gives the most accurate information on the timing because it is directly derived from the quantity itself. Unfortunately this approach has some drawback in case the statistics are very low. Especially when using a muon beam only the central channels have enough statistics to gather correct timing values. For this cases the timing can be monitored using LED calibration events which are fired during every spill. Their pulse is very wide, so the time cannot be calculated via a CFD but by calculating the center of gravity of those pulses. For many modules, especially those of Shashlik type, where the response on the LEDs is quite bad, and the pulses are very small. In that case a third method can be used for channels with a big difference in the even and odd baselines. There the pedestal values can be compared to a reference and if the two values switch, a jump has occurred. This method does not allow to correct the jump, because it only shows that a jump occurred, but not in which direction.

Also the timing of the trigger over the different interfaces should be monitored. On the carrier card, one could store the spectrum of the sum to the data stream of the corresponding event. This would allow to compare the sum value with the sum value calculated offline. If the interfaces are synchronous, these two quantities have to be identical. A similar method could be used if we connect the backplane to the readout, and also store the energy spectrum. For this a possible implementation still has to be discussed.

In order to also be safe in determining the correct amplitude, there has to be a monitoring of the amplitudes determined by the CFD in the FPGA compared with the amplitudes

determined offline. For that the data is already stored in the data stream of each channel, but no implementation exists in the online monitoring tools so far.

To combine all the information from the trigger, there should be a separate tool for ECAL2 trigger monitoring. This tool should be able to decode the data stream as well as being able to read out the VME registers from the GeSiCAs. This tool does not exist and has to be developed until the next run where the trigger system will be used.

Chapter 6

Conclusions and Outlook

For this thesis a digital trigger for the electromagnetic calorimeter in the second stage of the COMPASS experiment has been developed. Having several complications while commissioning it during the running experiment the final set up was completed on November 7th 2009. After that 10 data were taken for 10 days with an amount of nearly 10,000 recorded spills. Analysis of the trigger showed two problems in amplitude determination and timing which are understood and solved. Despite of that the trigger concept was proven and the system can be used during the planned full year of Primakoff data taking in 2012. The trigger system will be completed until then covering the full detector area and thus can be set up in any configuration concerning trigger area and thresholds. Extrapolated trigger rates are shown in figure 6.1 as a function of thresholds for the current area used as well as a function of the area for both thresholds used during the 2009 run (Fig. 6.2). Having a freely configurable set up of the trigger also the possibility of implementing amplification factors depended on the position in the calorimeter is under discussion. This would allow to adapt the trigger to the energy-angle dependence of the cross section of the process one wants to study.

Further the backplanes provide the possibility to implement communication between all the carrier cards. This allows to implement a cluster finding algorithm for the calorimeter which is planned to use as a method of zero suppression. This will allow to increase the threshold and therefor to select only the main cells of a cluster. The surrounding cells will then get a smaller threshold depending on their distance to the main cells. This method shall reduce the noise contribution to the recorded signals and at the same time increase the energy resolution of the individual clusters. For this the next development stages will be to move the zero suppression algorithm currently used from the mezzanine card FPGA to the carrier card FPGA. And in the next steps simulation and development of the clustering code will be done.
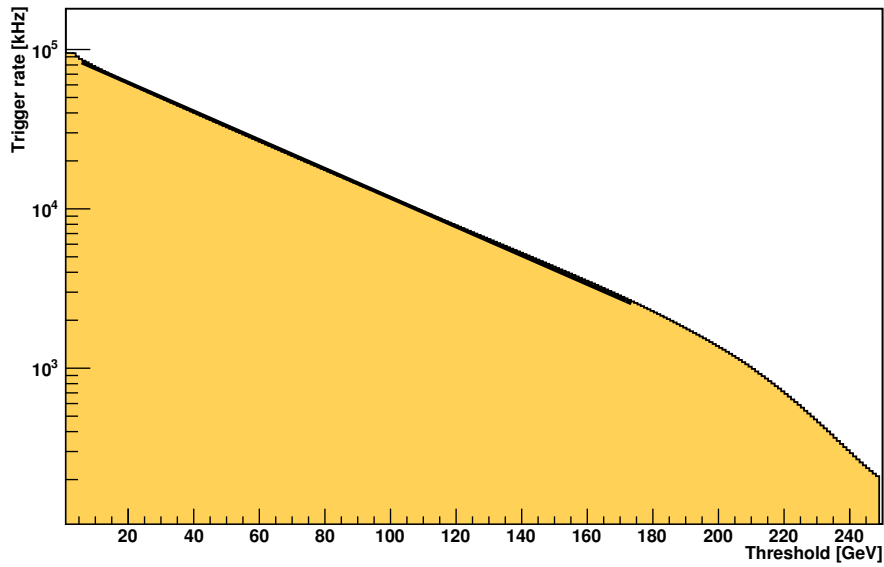
Figure 6.1: Threshold dependence of the trigger rate for the area selected in 2009. Plotted in logarithmic scale. The slope is fitted with an exponential function which matches over nearly the whole energy range.
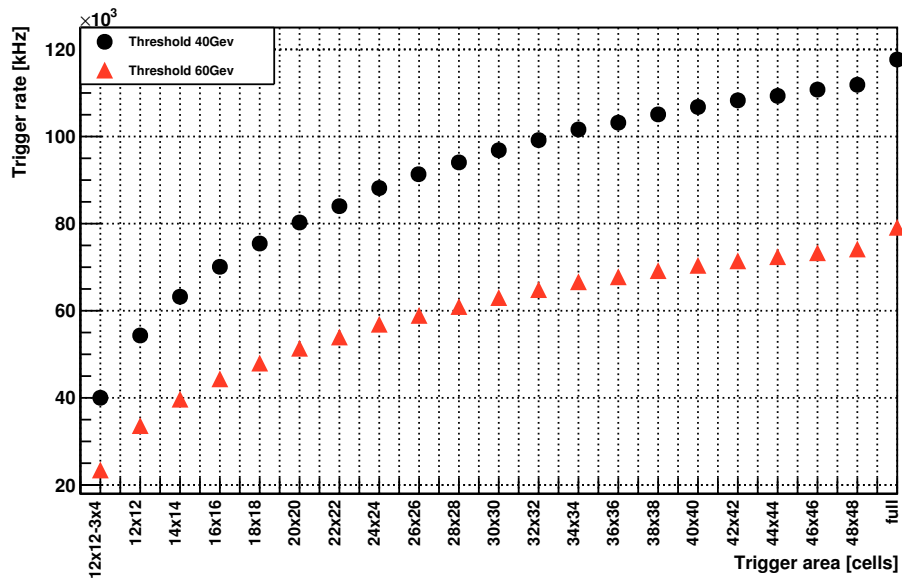

Figure 6.2: Dependence of the trigger rate on the selected area for different thresholds.

List of Figures

List of Tables

Bibliography

[1] P. Abbon et al. The compass experiment at cern. *Nucl. Instrum. Methods Phys. Res., A*, 577:455–518, Jan 2007. (Cited on pages 3, 7, 8, 9, 10, and 11.)

[2] The COMPASS collaboration. Compass-ll proposal. 2010. (Cited on pages 1 and 6.)

[3] J. Friedrich, S. Huber, B. Ketzer, M. Kramer, I. Konorov, A. Mann, and S. Paul. A digital calorimetric trigger for the compass experiment at cern. In *TWEPP-09: Topical Workshop on Electronics for Particle Physics*, pages 182–185, 2009.

[4] B. Grube. *A Trigger Control System for COMPASS and a Measurement of the Transverse Polarization of* Λ *and* Ξ *Hyperons from Quasi-Real Photo-Production*. PhD thesis, TU München, Physik-Department E18, 2006. (Cited on page 17.)

[5] A. Mann, A. M. Dinkelbach, B. Grube, B. Ketzer, F. Haas, H. Angerer, I. Konorov, J. Friedrich, M. Krämer, S. Grabmüller, S. Huber, S. Paul, and S. Uhl. The universal sampling adc readout system of the compass experiment. In *IEEE Nuclear Science Symposium*, pages 2225–2228, 2009. (Cited on page 16.)

[6] A. Mann, I. Konorov, and S. Paul. A versatile sampling adc system for on-detector applications and the advancedtca crate standard. In *15th IEEE-NPSS Real-Time Conference*, 2007. (Cited on page 19.)

[7] XILINX. Virtex-4 fpga user guide. (Cited on pages 22 and 47.)

Appendix A

A.1 Division lookup table

Input	Output	Input	Output	Input	Output	Input	Output
0	127	16	64	32	32	48	21
1	127	17	60	33	31	49	21
2	127	18	56	34	30	50	20
3	127	19	53	35	29	51	20
4	127	20	51	36	28	52	20
5	127	21	48	37	27	53	19
6	127	22	46	38	27	54	19
7	127	23	44	39	26	55	18
8	127	24	42	40	25	56	18
9	113	25	41	41	25	57	18
10	102	26	39	42	24	58	18
11	92	27	38	43	24	59	17
12	85	28	36	44	23	60	17
13	78	29	35	45	23	61	17
14	73	30	34	46	22	62	16
15	68	31	33	47	22	63	16

Table A.1: The lookup table for $1/x$. Here x is limited to a range of 6 bits where $1/x$ is defined as a 7 bit value defined by $1/x*1024$ where only the integer part was taken. For values of x smaller than eight the value is saturated at 127.

A.2 MSADC configuration registers

Address	Description	writable?
0x0000	Latency in clock cycles	yes
0x0001	Number of samples	yes
0x0002	Firmware version	no
0x0003	Mode of data writing	yes
0x0004	Start index of summation 0	yes
0x0005	Number of samples to sum up for sum 0	yes
0x0006	Start index of summation 1	yes
0x0007	Number of samples to sum up for sum 1	yes
0x0008	Start index of summation 2	yes
0x0009	Number of samples to sum up for sum 2	yes
0x000A	CFD amplification	not used
0x000B	Width of the window for amplitude scan	yes
0x000C	Baseline value for the readout	yes
0x000D	CFD threshold	yes
0x000E	CFD delay	yes
0x001$\underline{i}$	Threshold for channel i (i=0x0-0xF)	yes
0x0020	DAC value (offset of the ADC)	yes
0x0021	AVR firmware version	no
0x0022	ADC temperature	no
0x0030	spi_addr	yes
0x0031	spi_data	yes
0x004$\underline{i}$	Time constant for channel i (i=0x0-0xF)	yes
0x005$\underline{i}$	Energy calibration coef. for channel i (i=0x0-0xF)	yes
0x0060 - 0x007F	CFD hit counter for all channels / always two addresses form one 32 bit word for one channel	no

0x0080 -	pedestal values for all channels	no
0x009F	even addresses for even channels odd addresses for odd channels	
0x0100	I^{2}C test register (no internal meaning)	yes

Table A.2: Configuration registers for the MSADC card.

Bit	Name	Description
0	Sparse mode	needed for default data format
1	Extended Sparse mode	needed for default data format
2	Truncate mode	don't write data
3	Invert mode	inverts polarity of the pulse
4	Min-Max Trigger	Zero Suppression on maximum and minimum
5	Pedestal Trigger	Zero Suppression of sum in window 1
6	Mark only	No zero suppression only marking
7	Pedestal mode	Pedestal subtraction for the readout data
8	TDC mode	(not used)
9	Pedestal max trigger	Zero Suppression on the maximum over the fixed baseline

Table A.3: Description of the data mode register (0x0003).
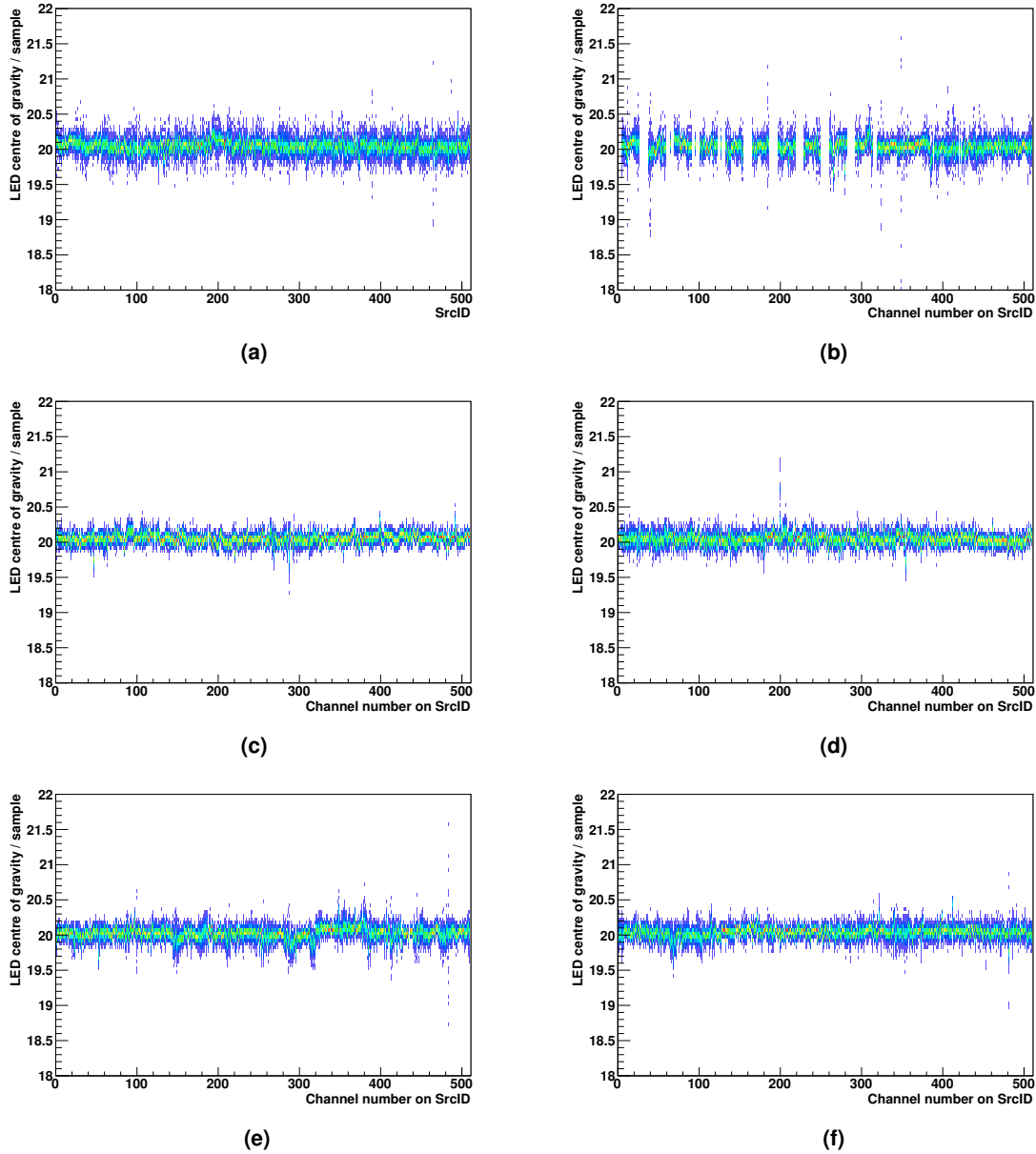
A.3 Time Monitoring During the 2010 Run

Figure A.1: Monitoring of the time stability of ECAL2 with the LED calibration pulses. The time is calculated via the center of gravity of all 32 samples. The wider shape in SrcID 616 and 617 comes from the bad LED coupling of the Shashlik modules.
SrcIDs: a) 616 b) 617 c) 618 d) 619 e) 620 f) 621

Appendix B

Acknowledgements

At first I would like to thank Prof. Stephan Paul for giving me the possibility to work at his chair on this exciting topic.

Next I would like to thank Igor Konorov for proposing this work as well as supporting me during the whole development by feedback as well as personal work on the project. The discussion with him during the analysis period were always very productive.

Further I would like to thank Alexander Man for developing the MSADC cards and for giving answers to many questions concerning the VHDL code. He supported me also very much during the implementation of the 160 MHz interface.

Many thanks also go to Markus Krämer and Thiemo Nagel. Markus for developing the algorithm and providing the software necessary for getting the trigger running and Thiemo for assisting during the final tuning and commissioning.

I am also very grateful to Florian Haas who gave me psychological support during a time where I stopped believing in a successful completion in 2009.

I am also much obliged to Svenja Lippok who did the final checks to this thesis.

Finally want to thank my parents for supporting me through my whole studies.